Investigation of Left Ventricle Flow Dynamics in the Presence of Mitral Annular Calcification

Batoul El-Sayegh

A Thesis

in the Department of

Mechanical, Industrial and Aerospace Engineering

Presented in Partial Fulfillment of the Requirements
for the Degree Master of Applied Science (Mechanical Engineering)
Concordia University
Montreal, Quebec, Canada

September 2017

© Batoul El-Sayegh, 2017

CONCORDIA UNIVERSITY

School of Graduate Studies

This is to certify that the thesis prepared,

By: **Batoul El-Sayegh**

Entitled: **"Investigation of Left Ventricle Flow Dynamics in the Presence of Mitral Annular Calcification"**

and submitted in partial fulfillment of the requirements for the degree of

Master of Applied Science (Mechanical Engineering)

complies with the regulations of the University and meets the accepted standards with respect to originality and quality.

Signed by the Final Examining Committee:

_____ Chair
Dr. T. H. Kwok

_____ Examiner
Dr. C. B. Kiyanda

_____ Examiner
Dr. A. Bhowmick CIISE External

_____ Supervisor
Dr. L. Kadem

Approved by: _____
Dr. S. Narayanswamy, MASc Program Director
Department of Mechanical and Industrial Engineering

_____
Dean Amir Asif
Faculty of Engineering and Computer Science

Date:_____

To

the ones

who sacrificed

guided, encouraged & loved unconditionally

to my greatest bliss

to my parents

Iman & Ali

ABSTRACT

Mitral Annular Calcification (MAC) is a degenerative heart disease corresponding to a deformation and narrowing of the mitral valve. Up to 42% of people aged over 65 have it, and 60% of people aged over 85. The aim of the present work was to understand the flow downstream of a calcified valve and to investigate how both the severity and the orientation affect the characteristics of the velocity field, vorticity field, viscous energy loss, vortex formation time, viscous shear stress, particle path, and shear accumulation.

For the purpose of this experimental thesis, particle image velocimetry was conducted at physiological flow and pressure conditions in two stages. The first stage is the *in vitro* experiment with seven different mitral valve configurations: (1) normal, (2) mild, (3) moderate with two orientations, (4) severe with three different orientations. Results show that compared with a normal case the instantaneous velocity, vorticity, and shear stress fields in addition to the energy loss evolution and vortex formation time significantly increase with MAC severities. It also showed, that keeping the same severity but modifying the orientation of the mitral valve also significantly lead to sub-optimal hemodynamic configurations.

Findings of this study indicate that the presence of MAC and orientation in the mitral valve significantly alters the hemodynamics in the left ventricle. This study sheds some light on the crucial rule that the orientation of the mitral valve plays in the severity assessment.

The second stage is experiments with models of patient specific valves with three different configurations (1) normal, (2) moderate MAC and (3) severe MAC. Results show that compared with a normal case the velocity and vorticity fields increased with MAC severities. Interestingly, it also showed, that the moderate case had higher averaged energy loss than that of the severe case. The energy loss of the severe was even less than that of the normal.

In conclusion, this study advances the current state of understanding of flow through calcified mitral valve by investigating how MAC affects the hemodynamics in the LV. Results can be used as the foundation for further investigations in order to better clinically evaluate mitral annular calcification.

ACKNOWLEDGEMENT

First and foremost I would like to thank Dr.Lyes Kadem for the opportunity to work under his supervision. He is such an enthusiastic, passionate, and knowledgeable supervisor. His guidance helped me throughout the research and thesis writing. I'm thankful for each opportunity he has granted me to grow education and skill wise.

I would like to thank Dr.Gregg Pressman and Dr.Edinrin Obasare, our collaborators from Einstein Medical Center, for providing us with the original idea, the 3D patient-specific valves along with their STL images, and for their continuous medical guidance and suggestions through the thesis.

My sincere thanks to my lab mates especially Dr.Hani Abulkahir and Giuseppe Di labbio at LCFD at Concordia for the knowledge exchanged. The lab was a place to learn, develop, and scout talents.

Last but not the least, my sincere thanks goes to my family without whom I wouldn't be able to be where I am. My parents Iman and Ali, no word can describe my gratitude to your continuous sacrifice, motivation, and unconditional love throughout every stage of my life. My warmest appreciation to my bigger sister Zeinab. Her incredible smartness and support guided my way. My deepest gratitude to my sisters Mahasen, and Fatima, and my brother Abbass, who filled my days with joy and happiness.

TABLE OF CONTENT

LIST OF FIGURES

LIST OF TABLES

SYMBOLS

α	Magnification factor (pixels/mm)
Ar, Ak	Constants for Richardson extrapolation
dt	Exposure time (s)
l_r	Distance of reference point (mm)
L_r	Distance of reference image (pixels)
l_t	Distance from the target (mm)
t	Time (s)
τ	Viscous shear stress (Pa)
u	Velocity vector component across x-axis (m/s)
μ	Fluid viscosity (Pa.s)
v	Velocity vector component across y-axis (m/s)
V	Velocity magnitude (m/s)
ω	Vorticity (1/s)
x, y	Spatial Coordinates (mm)

ABBREVIATIONS

AR	Aortic Regurgitation
CHS	Cardiovascular Health Study
CT	Computed Tomography
D	Dimensional
EL	Energy Loss
EPI	Energetic Performance Index
ESRD	End Stage Renal Disease
LV	Left Ventricle
MAC	Mitral Annular Calcification
MPW	Mean Platelet Width
MRI	Magnetic Resonance Imaging
MS	Mitral Stenosis
MVP	Mean Platelet Volume
PAS	Platelet Activation State
PIV	Particle Image Velocimetry
RBC	Red Blood Cells
SA	Shear Stress Accumulation
SJM	Saint Jude Medical

STL STereoLithography

VFM Vector Flow Mapping

VFT Vortex Formation Time

VSS Viscous Shear Stress

CHAPTER 1: INTRODUCTION

1.1 Overview of the heart

For every functional system there should be a control center, soldiers, and a supplier. As for the human body, the brain is the control, the organs are the soldiers, and the heart is the supplier. The heart is a muscular organ, which keeps all body organs alive by supplying them with blood carrying their needs of oxygen and nutrients. This supplying role is achieved by the heart acting as a continuous sophisticated pump, where each beat represents a complete cardiac cycle that takes around 0.85 seconds accounting for 70 beats per minute (Vander et al. 1975).

The heart can be divided longitudinally into left and right heart, each consisting of an atrium, a ventricle, and two valves. The right heart is composed of the right atrium, tricuspid valve that connects the right atrium to the right ventricle, and pulmonary valve which connects the right ventricle to the pulmonary artery. Similarly, the left heart consists of the left atrium and left ventricle connected by the mitral valve, and the aortic valve connecting the left ventricle to the aorta (Fig. 1-1).

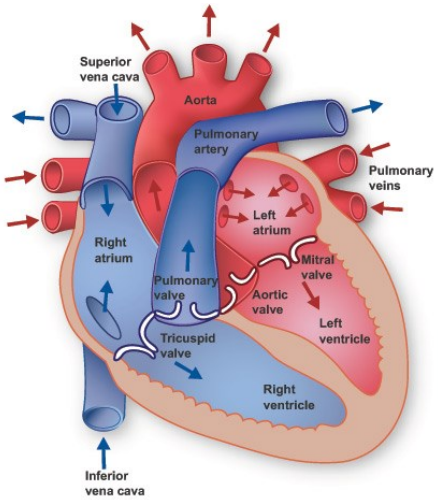

Figure 1-1 Healthy human heart anatomy [1].

The left heart is more subjected to diseases than the right side, due to greater pressures carried within. During systole the mitral valve carries a pressure of 150 mmHg, the aortic valve carries a pressure of 100 mmHg, while the tricuspid and pulmonary valve carry a pressure of 30 mmHg (Yoganathan et al. 2004).

Blood flows from regions of higher pressure to regions of lower pressure, which is the major principle for blood flow in the heart. Since the major role of the heart is to pump blood to the organs, this is accomplished by the fluid pressure created by cardiac contractions. The heart valves serve to direct the flow, preventing any opposing movement to that required.

The cardiac system is divided into two circulations; the pulmonary circulation that circulates the deoxygenated blood from the heart to the lungs done by the right heart, and the systemic circulation which takes the blood from the heart to the organs, tissues, and cells done by the left heart.

A cardiac cycle consists majorly of systole (ventricle contraction) and diastole (ventricle relaxation), as seen in Fig. 1.2, occurring in the following manner:

1- In late diastole, both the left ventricle, and atrium are relaxed, the blood pressure in the atrium is slightly higher than that of the ventricle due to blood entering to the atrium from the pulmonary veins. The mitral valve is opened, allowing the filling of the ventricle. Atrium then contracts adding a small amount of blood to the ventricle. Here the aortic valve is closed.

2- In systole, the ventricle contracts causing pressure to increase sharply, which allows blood flow from the left ventricle to the aorta through the aortic valve, then to all body organs from there. Here the mitral valve is closed to prevent any backward flow.

3- The right heart undergoes the same procedure as the left heart.

4- The volume of the blood pumped by the ventricles is the same, else there is a disease.

5- The systole consists of 1/3 of the cardiac cycle while the diastole consists of the remaining 2/3, under normal conditions.

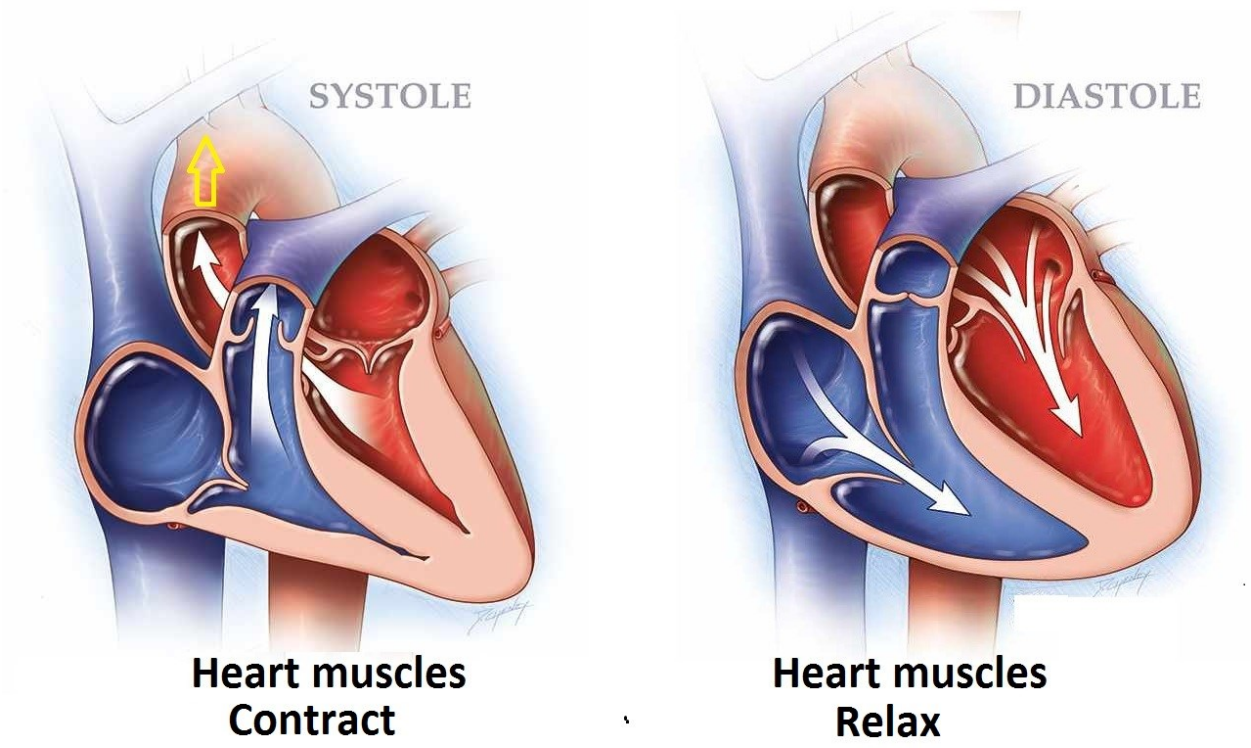

Figure 1-2 (a) Ventricular Systole (b) Ventricular diastole [2]

1.2 Heart Disease

Valvular calcification

One of the diseases that can affect the heart valves is calcification. Calcification is the condition where the valve deforms in shape and size due to calcium deposits accumulating on it (Fulkerson et al. 1979). These deposits cause the thickening of the valve leaflet and the narrowing of the valve. Valvular calcification is frequent with aging and diverse diseases. It can affect any valve in the heart, but clinical reports have indicated that the calcification for the left heart valves is more

common than the calcification of those of the right heart (Harpaz et al. 2001). This might be explained by the differences in carried pressures mentioned before.

Mitral Annular Calcification (MAC)

Mitral Annular Calcification (MAC) is a degenerative process where the fibrous annulus of the mitral valve degrades, causing both deformation and decrease in the geometrical orifice area of the valve (Fig. 1-3& Fig. 1-4). The area can be reduced from 4-5 cm^2 in normal patients to less than 1 cm^2 in patients with severe MAC. MAC is a chronic disease, that doesn't heal completely but stays with the person throughout his/her life.

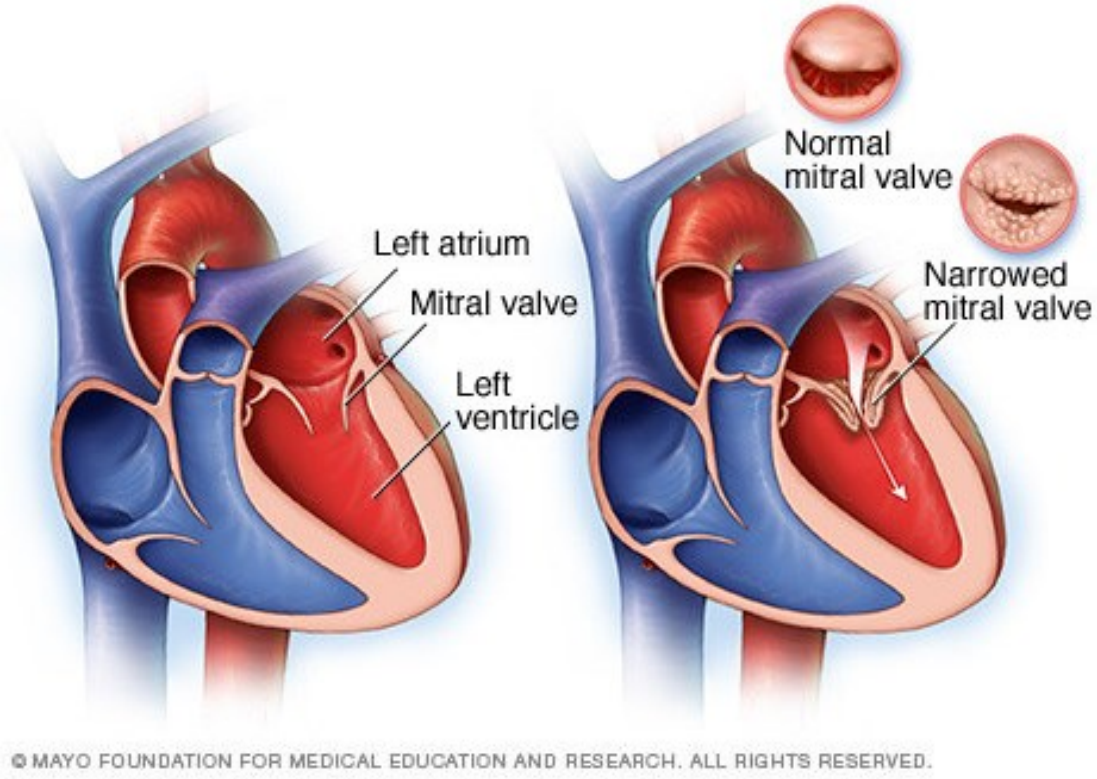

Figure 1-3 Normal vs narrowed mitral valve [3]

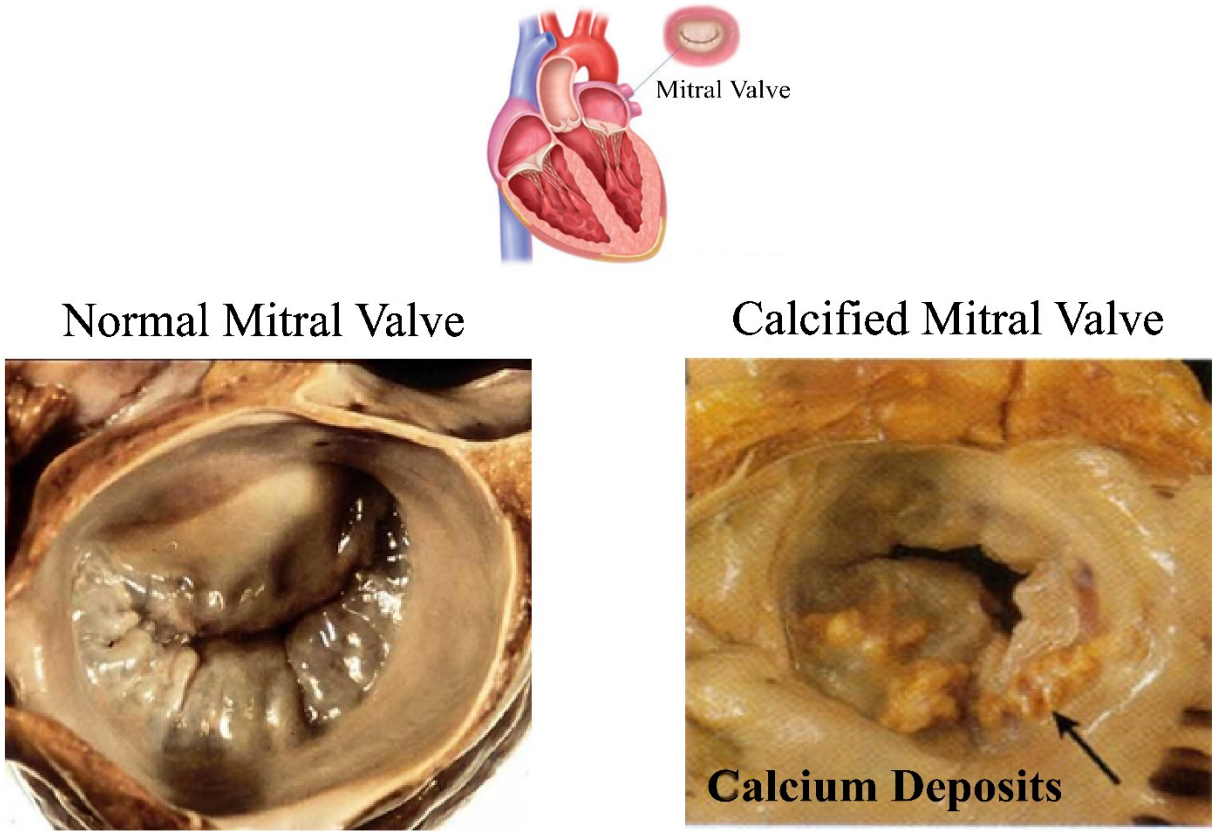

Figure 1-4 Normal vs calcified mitral valve [4, 5, and 6]

The prevalence of MAC increases with age. Considering both middle age and elderly population, the prevalence of MAC is estimated to be around 9% (Kanjanauthai et al. 2010). Furthermore, in the cardiovascular health study CHS, a study on elderly population, MAC was found in approximately 42% of people aged over 65, and in 60% of people aged over 85 (Barasch et al. 2005).

MAC has no visible symptoms, it is an incidental finding on echocardiography. It has no treatment until now, the way doctors manage this disease, is by treating the associated diseases and conditions caused by MAC. In some severe MAC cases the mitral valve needs a surgical

replacement. Such surgical procedures need critical evaluation, and have high mortality rates due to the complications caused by MAC (d'Alessandro et al. 2007; Feindel et al. 2003).

1.3 Diagnosis

The discovery of MAC happens as an incidental finding mostly on echocardiography. There are different ways to diagnose MAC all depending on capturing an image of the heart which will allow to identify this disease. The difference in the methods is in the capability of distinguishing MAC from other diseases, and specifically identifying its severity. Previously, echocardiography was the most common way to diagnose MAC. Nowadays, the use of computed tomography is being more encouraged.

- ***Echocardiography.*** The most common way to identify MAC presence is by echocardiography. The image shows unusual white deposits on the posterior annulus of the valve, described as an echo-dense shelf like structure, associated with acoustic shadowing. The drawback of echocardiography is that it has relatively low distinguishing rate between MAC and dense collagen (Kanjanauthai et al. 2010), yet it remains the easiest and cheapest way of all ways presented.
- ***Chest x-ray.*** In severe cases, MAC might appear on chest x-rays. The fact that this method cannot identify MAC in all its severities, makes it neither reliable nor practical to be used for diagnosis.
- ***Fluoroscopy.*** MAC can be shown in fluoroscopy. The limitation of this method is its low rate in correctly identifying the extent of MAC, and as a result its severity.

  Both chest x-ray and fluoroscopy are radiation based diagnosis. There is a limited amount of radiation allowed for the human body, else, risk of cancer is raised, causing these two methods to be unpractical methods for MAC diagnosis.

- ***Computed Tomography (CT).*** It is the most recently growing method, due to its ability to identify the extent, location, and severity of MAC with no drawbacks recorded.

- ***Magnetic Resonance Imaging (MRI).*** Magnetic resonance imaging is less popular for identifying MAC, since calcium is hypo-intense (Dark on MRI image) compared to myocardium (Gulati et al. 2011).

1.4 *Consequences of MAC*

The importance of MAC lies in the cardiovascular diseases and complications occurring in association with it, from which is coronary heart disease, carotid artery stenosis, conduction system disease, and atherosclerosis of aorta. MAC more significantly doubles the risk of stroke (Benjamin et al. 1992), and increases the risk of mortality and cardiovascular events. In the Framingham Heart Study (Fox et al. 2003), it was found that with a 1 mm increase in the thickness of MAC, the risk of cardiovascular diseases and cardiovascular death incidence increases by 10 %, and the risk of stroke increases by 1.24%. Notice that the thickness of a diseased mitral valve can reach up to 10 mm (5 mm increase above normal thickness).

1.5 Thesis Structure

Purpose of this study

Normal flow patterns within the Left Ventricle (LV) optimize energy efficiency. Cardiac disease leads to disturbed flow and suboptimal LV performance. Although some studies have investigated the possible existence of cause-effect relationship between MAC and other diseases such as mitral stenosis (Pressman et al. 2009), mitral regurgitation (Osterberger et al. 1981; Labovitz et al. 1985; Aronow et al. 1987; Movahed et al. 2007), atherosclerosis (Kanjanauthai et

al. 2010). However, to the best of our knowledge there is no study exploring the effects of MAC on LV flow patterns and hemodynamics.

MAC has currently low positive predictive value. By revealing the effects of MAC severities on the blood flow in LV, we can relate MAC to cardiovascular related symptoms which will help diagnose this disease at early stages.

The aim of this work is to investigate the effects of MAC on the left ventricle hemodynamics and flow patterns, in order to develop new clinical parameters. This is done through an in vitro study performed using custom made double pulse heart duplicator with different MAC severities and mitral valve orifice area orientations under the same physiological conditions.

Organization of this thesis

This thesis will be presented in the following sequence; in chapter 2, a literature review will be conducted on the optimized flow in the left ventricle, followed by a brief summary of the available data present in the literature about MAC flow in the LV. Then, in chapter 3, a full description of the method used in the experiments is offered. Chapter 4 will present the results of the experimentations and they will be discussed. Finally, a conclusion will summarize the results along with the limitations and possible future work directions.

CHAPTER 2: LITERATURE REVIEW

Several works have investigated the flow dynamics in the left ventricle under healthy condition. The main objective being stating reference normal values for pathological heart conditions. For this reason, several studies have introduced different parameters from velocity magnitudes, vortex formation number, shear stresses, shear accumulation and energy loss in order to quantify the optimized flow patterns in the left ventricle. However, only few studies investigated diseased cases and showed how pathological flow patterns diverge from the normal flow patterns.

2.1 *Velocity and Vorticity Fields in the Left Ventricle*

The velocity and vorticity fields have been the most reported parameters throughout the literature due to the feasibility of acquiring these parameters with the development of different methods *in vivo*, such as vector flow mapping (Garcia et al. 2010; Itatani 2013; Stugaard et al. 2015; Akiyama et al. 2017; Hong et al. 2008; Martinez-Legazpi et al. 2014), and MRI (Gharib et al. 2006). *In vitro*, particle image velocimetry (Tanne et al. 2009; Falahatpisheh and Kheradvar 2012) and numerical simulations (Pedrizzetti et al. 2005; Domenichni et al. 2006; Watanabe et al. 2008: Arefin et al. 2014) are used along with other techniques. A good physical description of flow dynamics in the left ventricle can be found in the book "**Vortex formation in the cardiovascular system"**. The third chapter of this book summarizes a part of the previous studies in the field regarding the trans-mitral inflow and vortex characteristics in the left ventricle. The trans-mitral flow was described as a laminar flow, with usually low velocity (less than 100 cm/s). The filling is divided into two phases; the E and A-wave. The E-wave phase is during early diastole upon the relaxation of the ventricle and due to pressure difference between the left atrium and the left ventricle, while the A-wave is during atrial systole upon the contraction of the left atrium. The velocities for the E-wave are slightly higher than those of the A-wave. Regarding the trans-mitral

vortex, it was initially reported in an *in vitro* study of the left ventricular flow (Bellhouse 1972; Reul et al. 1981) and then confirmed by a color Doppler mapping (Kim et al. 1994), and MRI (Kim et al. 1995; Kilner et al. 2000). The vortex is driven by a strong jet and recent studies reported that the vortex tends to be asymmetric due to the asymmetry of the mitral valve leaflets. Lastly, the authors discussed the factors affecting the left ventricle vortex. The vortex is affected by several factors, namely, the saddle annulus dynamics (by modifying the length of the leaflets), and the angle of valve opening which influences the flow-wall interaction causing changes in the stability, dynamics, and shape of the vortex formed (Kheradvar and Falahatpisheh 2012).

As for MAC, a study in 2002 (Soeki et al. 2002) was performed on cohort including 53 patients with MAC, 30 normal patients, and 20 patients with hypertensive heart disease but no MAC. M-mode and two dimensional echocardiography was done to measure atrial and ventricle dimensions during different cardiac cycle moments. A pulsed Doppler echocardiography was applied to get the velocity waveforms. From the velocity waveform, the mitral orifice area was calculated. A pulsed Doppler tissue imaging was applied on the mitral annular area to get the velocities of its motion. A correlation between mitral inflow, mitral annular motion velocities and MAC was deduced. The study concluded that upon the increase of severities, consequently decrease in the mitral orifice area, the mitral inflow velocities increase respectively due to the restriction in the mitral annulus, while the mitral annular motion velocities decreased due to the abnormal left ventricle relaxation and limitation of mitral annular motion.

To the best of our knowledge only one study has evaluated the left ventricular velocities in patients with MAC.

2.2 *Viscous Energy Losses in the Left Ventricle*

In 2005, a study was performed by Pedrizzetti and Domenichini suggesting that nature optimizes the swirling flow in the human left ventricle. Numerical simulation for a pediatric left ventricle using pediatric clinical data was used to study the intraventricular flow. The asymmetry of the flow is altered by modification of the entering mitral jet. The results showed that the physiological vortex in the left ventricle other than helping in fast ejection of the flow, also minimizes the energy lost. The dissipation of energy increased by about 10% in the case of deviation from the physiological flow pattern that could be caused by several heart diseases or valve replacement. This increases the work of the heart muscles. Further studies (Bolger et al. 2007; Zhang et al. 2012; Zhang et al. 2013) emphasized the role of the vortex in decreasing the energy dissipation of flow in the left ventricle.

In 2008, a study was made by Watanabe et al., opposing that of Pedrizzetti and Domenichini (2005), where a heart model was developed using the finite element method. A physiological and a non-physiological inflow path were simulated. Flow fields were acquired showing the 3D flow motion. A comparison was made between the physiological flow path and the non-physiological one. A difference aroused from the blood leaving the heart. With an elevated heart rate, and after nine cycles, the whole blood would enter the left ventricle with the physiological inflow path, but with the non-physiological inflow path, about 27% of the blood remained in the left cavity. The conclusion from this work was that the physiological path does not save energy, but instead helps in the separation process between the inflow and the outflow. This is achieved by a looping procedure based on the first in first out mode rather than by flow mixing.

Several studies have tried to estimate the viscous energy loss (EL) for the flow entering the LV (Itatani et al. 2013; Hayashi et al. 2014; Honda et al. 2014). In 2013, a study was performed by

Keiichi et al. introducing a new method, which is vector flow mapping (VFM), allowing to determine different hemodynamic parameters in the heart. This VFM is a modification of the color Doppler method. The study showed the left ventricle streamlines, velocity, and viscous energy loss for several cases including normal case, following valve surgery, mechanical valve in anti-anatomical and anatomical positions, bioprosthetic valve, mitral valve plasty procedure and moderate and severe aortic regurgitation. This study gave useful measurements of EL in LV for some complicated cases.

Another study in 2015 (Stugaard et al. 2015) was performed aiming at quantifying the energy loss in the presence of aortic regurgitation (AR). For this, AR was induced in 11 dogs where VFM method was used to determine the viscous energy loss. This was followed by human recordings on 22 patients with AR and 12 normal cases. The study gave some EL values for AR cases.

However, the results have to be taken with caution because of inconsistencies in the units used for evaluating energy loss.

Two studies (Li et al. 2017; Zhong et al. 2016) used VFM to determine the energy loss fields for control cases *vs* patient cases. Both studies were clinical studies, where the energy loss was specifically compared during diastole and during systole. Li et al. 2017 investigated 88 diabetic patients and 58 healthy patients. The aim of the study was to use the energy dissipation as an index of the left ventricle function. The results showed a significant increase of diastolic and systolic EL in patients with uncontrolled blood glucose group ($p < 0.001$). Zhong et al. 2016 investigated the variations in the EL in 63 patients with end stage renal disease (ESRD) compared to 50 control cases. The aim was to determine the EL in the LV for ESRD patients. Both the diastolic and systolic EL were significantly higher in patients compared with control cases ($p < 0.001$).

In 2017, (Akiyama et al. 2017) used VFM to analyze the left ventricular energetic performance in 50 healthy adults. The aim of this study was to define reference values for the energy loss (Fig. 2-1), the kinetic energy and energetic performance index (EPI) for adults. Those parameters can be used clinically to evaluate various cardiac dysfunctions. The reference values were obtained, yet the EPI required further investigations because it is a new parameter introduced by this group.

To the best of our knowledge no study has evaluated the left ventricular energy loss in patients with MAC.

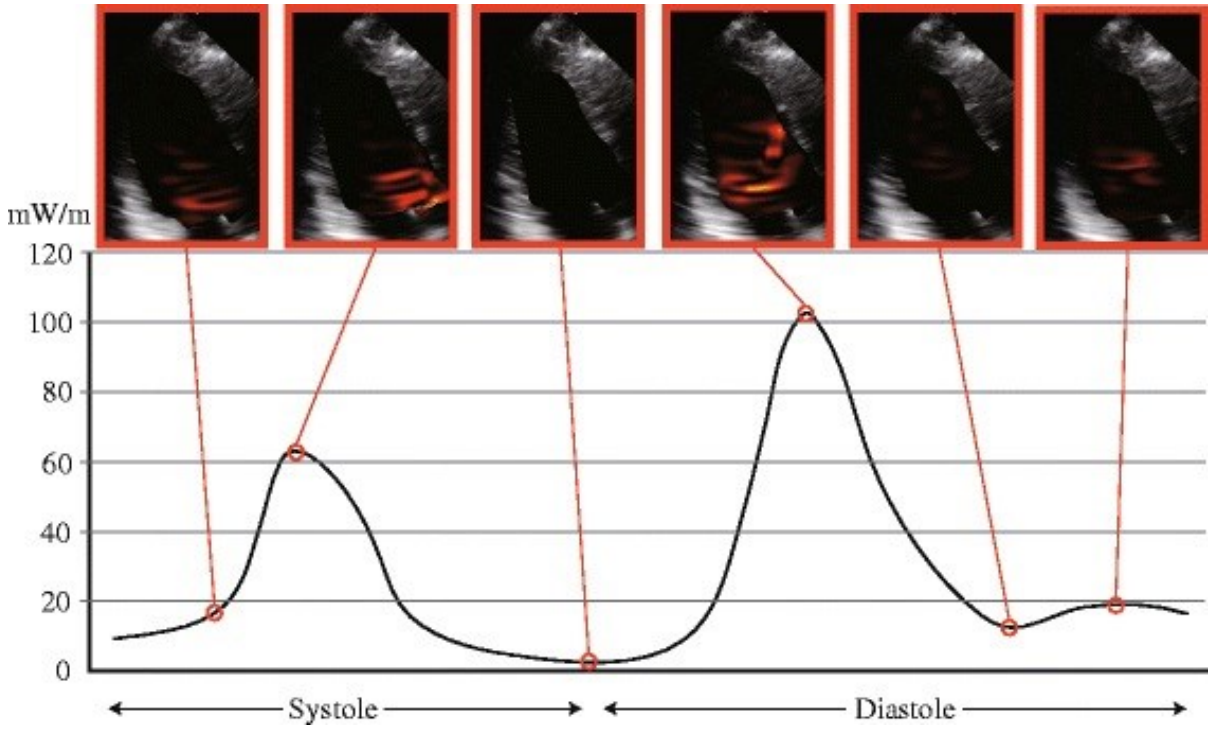

Figure 2-1 Energy loss images and graph of a healthy volunteer (Akiyama et al.2017 study)

2.3 *Vortex Formation Time*

In order to evaluate diastolic cardiac function, a dimensionless parameter was introduced to quantify the efficiency of the vortex formed during the diastolic filling in the heart. An equation

was introduced and validated through *in vitro* and in vivo experiments. The optimal vortex formation time (VFT) range was found to be between 3.3 and 5.5 (Gharib et al. 2006).

Other groups suggested other formulations for the VFT leading to similar ranges for normal functioning conditions (Ghosh et al. 2009; Jiamsripong et al. 2009; Belohlavek et al. 2009; Poh et al. 2012; Ghosh et al. 2013).

Several studies have used the concept of VFT as an index of the left ventricle function to compare healthy and pathological conditions. In 2009, Jiamsrinpong et al. tested the hypothesis that VFT shifts from its optimal range due to LV afterload which impairs the flow efficiency. LV afterload was induced in 9 open-chest pigs. The results showed two important findings: 1) even a short moderate elevation in LV afterload causes a shift of VFT from its optimal range; 2) the VFT index is applicable independently of the species and the settings. (Gupta et al. 2011) calculated the VFT in patients with hypertrophic cardiomyopathy. They showed that VFT for patients with hypertrophic cardiomyopathy is lower than the optimal range. They suggested however that exercise activity may contribute towards a normalization of the VFT in those patients. For the control group, the VFT was 3.6±0.4, falling in the optimized expected range. However, (Agati et al. 2014) showed that patients with different stages of myocardial infarction do not have sub-optimal VFT values compared to normal patients.

In 2015, Pasipoilarides et al. objected on the concept that VFT is a universal index of ventricular function using data from two previous studies (Stewart et al. 2011; Stewart et al. 2012).

To the best of our knowledge no study has evaluated the vortex formation time in patients with MAC.

2.4 *Viscous Shears stress and Shear Accumulation*

When blood flow is subjected to elevated viscous shear stresses, blood platelets might get activated (Fig. 2-2). The consequence of platelets activation is the promotion of thrombus formation in the blood stream. A thrombus may prevent oxygen-rich blood flow from reaching the brain leading to risks of ischemic stroke

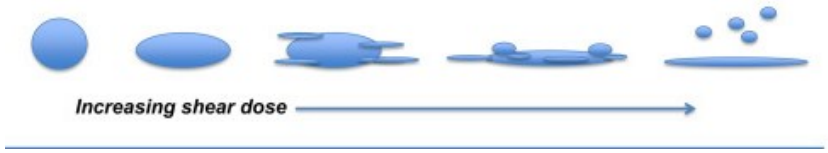

Figure 2-2 Platelet activation due to increase in shear ***(Slepian et al. 2016)***

Some studies have investigated the relationship between the mean platelet volume (MPV) with both thrombus (Gasparyan et al. 2011; Rupa-Matysek et al. 2014), and ischemic stroke occurrence (Bath et al. 2004; Mayda-Domac et al. 2010; ElSayed et al. 2017) due to platelet activation. The results show that MPV could be an indirect indicator of platelet activations. The value of MPV is identified as a predicative factor for thrombus reoccurrence in patients with antiphospholipid syndrome (Rupa-Matysek et al. 2014). Yet further investigations should be carried. On the other hand, MPV is suggested to be an early and imperative predictor of ischemic stroke (Mayda-Domac et al. 2010; ElSayed et al. 2017), and for patients of cerebrovascular disease with previous stroke history (Bath et al. 2004).

Some studies have calculated the wall shear stresses on the left ventricle to investigate their effect on endothelial cells (Itatani et al. 2013; McCormick et al. 2016; Zhang et al. 2017). Yet, most of the studies tend to show the viscous shear stress accumulation (SA), and the platelet activation state (PAS), the summation of the instantaneous shear multiplied by the exposure time

(Yin et al. 2004). The shear stress and exposure time are of a critical importance for the evaluation of SA (Zhang et al. 2003; Sheriff et al. 2013). PAS has been used to evaluate the platelet activation. A shear stress accumulation of 3.5 Pa.s is suggested as a threshold for platelets activation (Peterson et al. 1987).

As for MAC, only one study investigated platelet behaviors (Varol et al. 2012). This study evaluates in particular the mean platelet volume (MPV) and platelet distribution width (PDW) in the presence of MAC. This clinical study involved 101 patients with MAC, and 55 control subjects. The results show that MPV and MPW are significantly higher in patients with MAC ($p < 0.001$). Not only MPV and MPW were independently associated with MAC, but also positively correlated with atrial fibrillation, left atrial, and MAC. The study suggests therefore that patients with MAC have higher risks of thrombus formation.

In 2013, Balta et al. wrote a paper reviewing the study of (Varol et al. 2012). The paper suggests that the MPV alone is not enough to provide clinically relevant information on the endothelial cell inflammatory conditions. The evaluation of such a risk should be done using MPV coupled with another inflammatory marker such as C-reactive protein.

To the best of our knowledge no study has evaluated the shear stress, and shear accumulation, in patients with MAC.

As there are several clinical studies showing the prevalence and trying to relate MAC to other heart diseases in a cause-effect or partnership, studies concerning the velocity, energy loss, vorticity, vortex formation number, or shear accumulation of such mitral valve disease are still few, if not known. This is due to the difficulty in obtaining such parameters clinically through MRI, echocardiography, or other diagnosis methods. From an engineering point of view, left heart

simulators capable of getting such parameters are very limited, from which is the custom made experimental setup that we have in the lab. The importance of such investigation is in being first of its kind, opening the path and setting baselines for further research in this field.

CHAPTER 3: METHODOLOGY

This chapter will present the details of the experimental setup used for the purpose of this thesis, from elastic models painted and particle image velocimetry procedure to the uncertainty analysis used to calculate the error percentage.

3.1 *Left Heart Molds*

Realistic 3D printed models

CT patient specific images were obtained for the heart components. These files were converted to STL files. Then the models were 3D printed in the laboratory, and sanded to assure maximum smoothness required for the mold painting step.

Elastic models

Anatomical elastic models are usually used in a custom made experimental setup to replicate the heart components required for each experiment. In our experiment, and since we are considering only the left heart, models were made for the aorta, the left atrium and the LV (Fig. 3-1). In patient specific MAC cases tested, elastic models were made for the 3D printed valves.

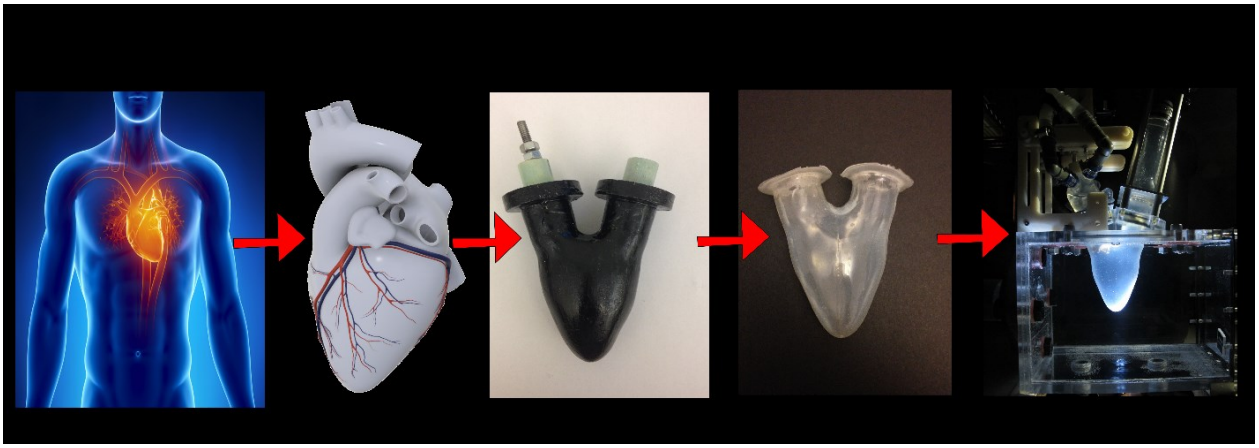

Figure 3-1 left ventricle silicone model creation steps [7].

The elastic models are made up of several layers of silicone mixture (MB Fiberglass Polycraft T-4 Translucent silicone Rubber 1.1kg kit). The silicone mixture consists of silastic T-4 base and a silastic T-4 curing agent as shown in Table 3-1. The mix ratio is 10:1; each 10 grams base with 1 gram curing agent. The number of layers used for each experiment depends on the stiffness needed for the specified physiological conditions. Increasing the number of layers, will increase the stiffness, thus making it less compliant. In our experiments, the number of layers used is chosen to be 5, as a compromise between elastic and optical properties.

After making the silicone mixture, the mixture is placed for around 30 minutes in a vacuum pump to remove air bubbles created upon mixing. Then using a paint brush, the 3D printed models are painted and placed in a rotating heater to dry with a speed of 21 rpm.

Table 3-1: Silicone mixture characteristics.

Characteristics	Value
Mix ratio	10:1
Tensile Strength MPa	6.7
Elongation at break %	400%
Tear Strength N/mm	26

3.2 *Blood Analogue*

Blood is a complex mixture of plasma, cells, platelets, and other elements. By volume, blood is composed of plasma (54.3 %), red blood cells (45%), and white blood cells accounting for 0.7%. Plasma acts as a Newtonian fluid at physiological rates of shear. On the other hand, red blood cells being the second effective component is highly flexible and deforms upon shear stress causing the viscosity to vary in some conditions. Considering the fact that the size of the red blood cells is

about 8 micron, studies have shown that upon having the size of the cavity being much larger than the size of RBC (> 1 mm), the fluid can be considered as a Newtonian fluid. Based on this, and since our study is on the left ventricle, the fluid is considered as Newtonian. For this purpose, the liquid used is a mixture of water 60% and glycerol 40% by volume to simulate the blood characteristics, where it has a dynamic viscosity of 3.7 cp and a density of 1100 kg/m^3 which is close to reported blood properties in large arteries (Waite and Fine 2007).

3.3 In Vitro Setup

Experimental apparatus

For the purpose of this thesis, a custom made double pulse duplicator capable of reproducing physiological and pathological conditions with anatomical elastic models of the aorta, left atrium and ventricle was used (Fig. 3-2).

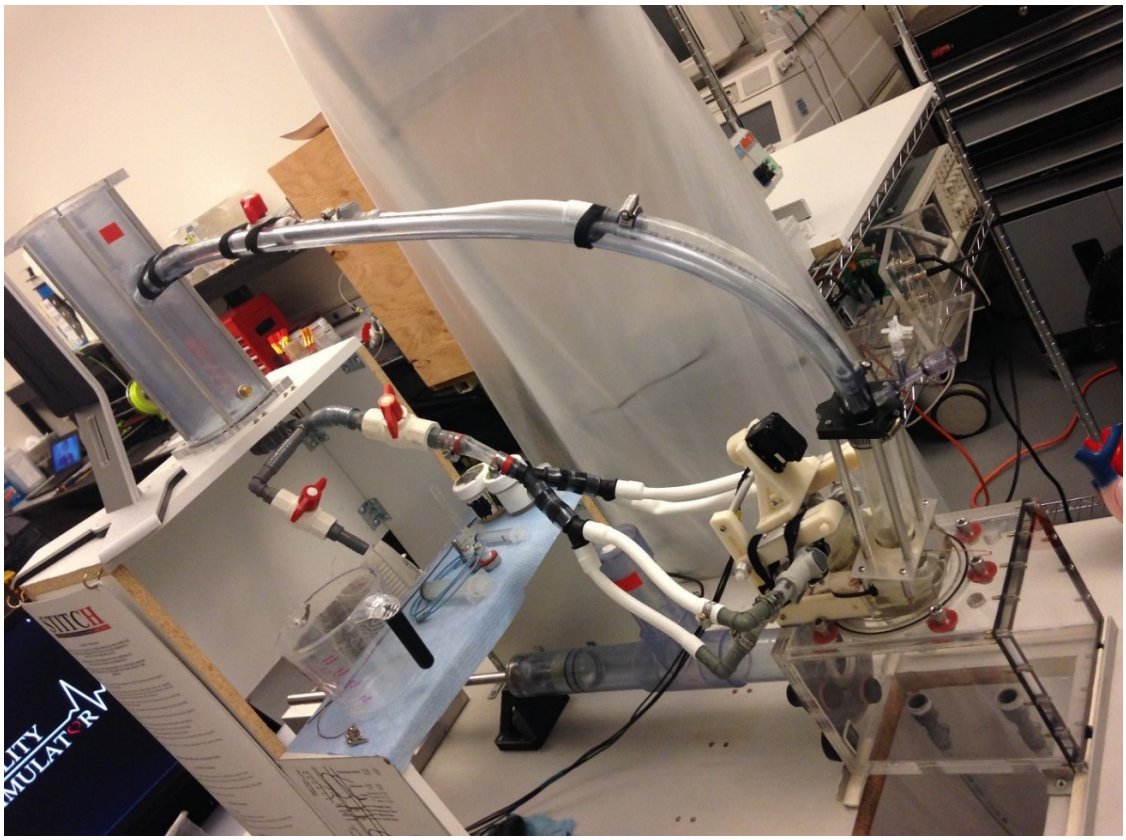

Figure 3-2 Experimental setup.

The duplicator consists of an open tank (reservoir) placed at the a higher level from other components, which supplies the fluid to the system, connected by tubes to the left atrium, which in turn is connected to the left ventricle by the mitral valve (25 mm Saint Jude Medical (SJM) porcine valve in the normal case). Left ventricle myocardium is simulated by a piston- cylinder assembly, which works according to a waveform supplied. We used a waveform that reproduces both E and A left atrium waves. The left ventricle in turn is connected to the aorta by the aortic valve (Biocor EDWARDS 25 mm prosthetic heart valve).Through the aorta, the fluid goes through tubes back to the main reservoir.

Two experiments were conducted on the same system, both experiments address the mitral valve, thus the only changes in the system are applied for the mitral valve. The first experiment is a fundamental study, to investigate the effect of the eccentricity and mitral orifice combined on the hemodynamics of the LV. For this purpose, the only thing modified in the system is that a rubber circular orifice was placed upstream the biological valve. Seven configurations were tested: normal, mild, moderate (2 cases), and severe (3 cases).

The second set of experiments are based on 3D patient specific mitral valves, obtained from our collaborators at Einstein Medical Center. Three configurations were tested: normal, moderate (Fig. 3-3), and severe. For the moderate and severe cases the silicone models painted from the 3D patient specific valves were sewed in the location of the mitral valve before testing.

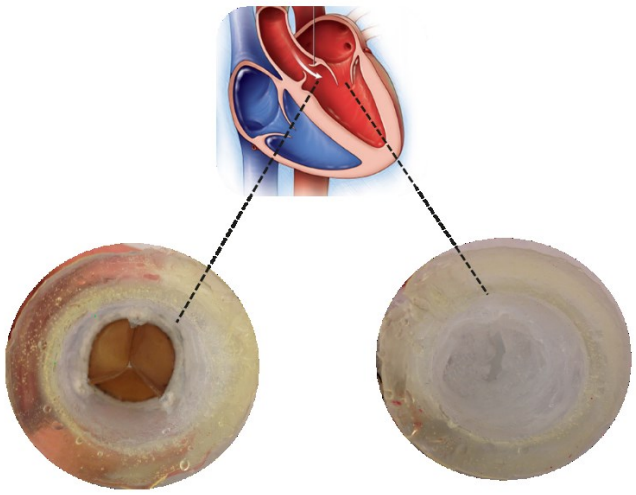

Figure 3-3 Prosthetic valve used as the aortic valve vs 3D patient specific silicone transparent valve tested in the mitral position [6].

Experimental conditions

The following conditions have been tested in this study: (1) normal mitral valve using a bioprosthetic valve with an orifice area of 4.91cm^2 (2) moderate MAC using a patient specific silicone model with orifice area of 1.17 cm^2 (3) and severe MAC using a patient specific silicone model with orifice area of 0.68 cm^2.

In the second set of experiments, the following configurations have been tested: (1) normal mitral valve using a bioprosthetic valve with an orifice area of 4.91 cm^2 (2) mild MAC having an orifice area of 2.54 cm^2 with one centered orientation, (3) moderate MAC with orifice area of 1.54 cm^2 with two possible orientations, (4) and severe MAC having an orifice area of 0.79 cm^2 with three possible orientations as shown in Fig. 3-4. The parameter *e* quantifies the orientation and is calculated by:

$$e = \frac{2 \times CC'}{D_0}$$

where C is the center of the outer diameter, C' is the center of the inner diameter, CC' is the distance between them, and D_0 is the outer diameter.

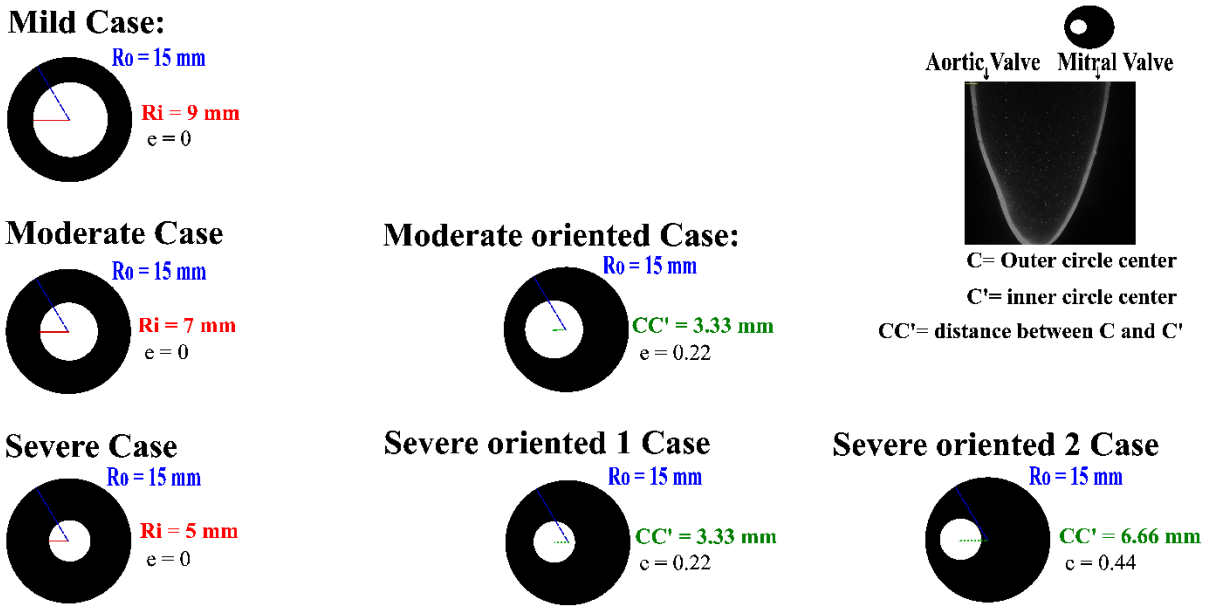

Figure 3-4 Orifice areas tested.

The aortic valve in all measured cases was the same tricuspid bio prosthetic valve (Biocor EDWARDS 25 mm prosthetic heart valve). The physiological conditions for all measurements were as follows: 70 bpm heart rate, 32 mm pump stroke, 70 ml stroke volume, 100 mmHg mean aortic pressure, and 5 L/min average flowrate

3.4 3D Patient Specific Valves Area

As we received a set of patient specific calcified mitral valves from Einstein Medical Center, the first step was to choose the valves to be tested. This process has been accomplished by evaluating the geometric orifice area of each valve and classifying them depending on the severity as defined by medical guidelines (Hatle and Angelsen 1985; Baumgartner et al. 2009) (Fig. 3-5). For this objective to be fulfilled, and with the complex orifice shapes, a simple area calculation was not feasible. This is why an image processing based procedure has been adopted.

Details of the procedure followed is presented in appendix A.

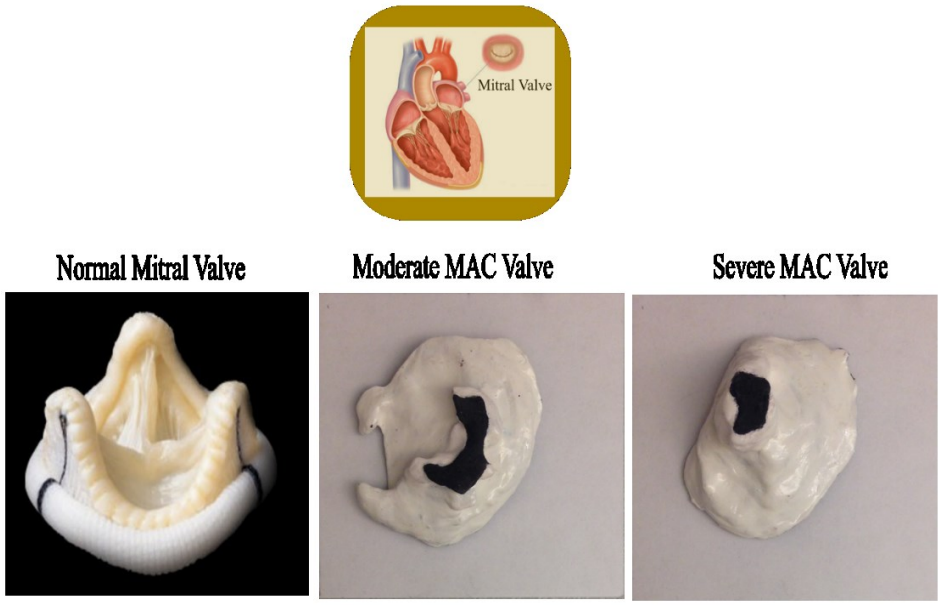

Figure 3-5: Mitral valves used for different cases [8].

3.5 *Particle Image Velocimetry*

Particle image velocimetry (PIV), is an optical technique used to get images for a fluid in motion. It is based on using a high speed camera, a laser beam, and seeding particles. The particles are fed in the fluid with the laser beam illuminating them. The camera takes two consecutive images spaced by a known short duration (*dt*). By knowing the time and distance the particle traveled, the velocity vectors can be calculated.

To calculate the different velocities of the countless particles shown in each image, the image is divided into interrogation regions varying typically between 8 and 64 pixels. Cross- correlation is applied then to calculate the velocities (speed with direction) of each particle. The process is accelerated by using fast Fourier transformation. PIV is applied in different research fields from biomedical (cardiovascular fluid dynamics), environmental (wave dynamics, coastal engineering), hydrodynamics (velocity measurement in water flows) to aircrafts (testing aerodynamics).

PIV system

PIV measurements were taken on the mid plane of the left ventricle (Fig. 3-6). A LaVision PIV (LaVision GmbH, Goettingen, Germany) system used in this study is composed of a dual cavity Nd: YLF laser (Litron lasers, Warwickshire, England) with a maximum repetition rate of 20 kHz and a maximum pulse energy of 10 mJ at 527 nm, and a Phantom v9.1 camera (Vision Research, Stuart, FL, USA) with 1,000 frames per second at a maximal resolution of 1,632 * 1,200 pixels. The laser was guided through an articulated laser arm. A thin laser layer was obtained (around 1 mm). Glass hollow spheres were placed in the fluid (mean diameter = 50 micrometers).

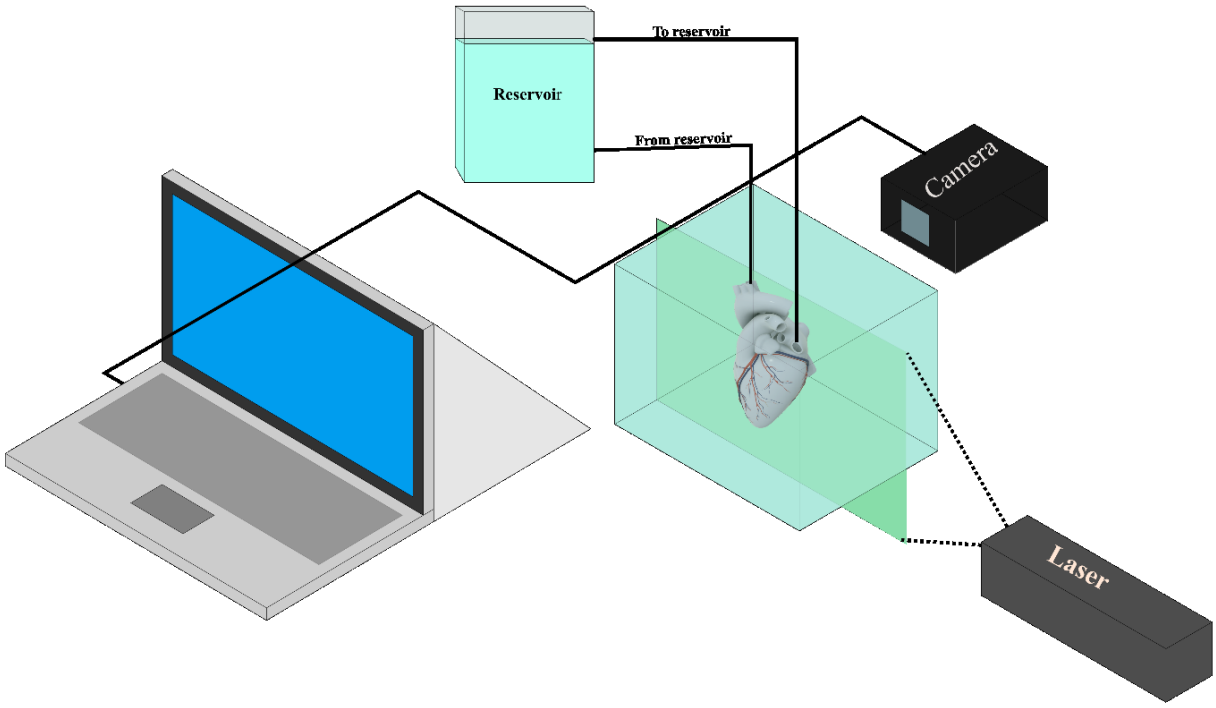

Figure 3-6 Schematic diagram for the experimental apparatus.

Table 3-2: PIV system specifications.

Laser	Nd: YLF laser (Litron Lasers, UK)
Camera	Phantom v9.1 camera (Vision Research, Stuart, FL, USA)
Camera Lens	Nikon AF Micro-Nikkor 60 mm f2.8D
Software	DaVis 7.2, LaVision GmbH, Germany

PIV setting

PIV settings were the same for all measurements. The *dt* parameter was selected in order to fulfill the one fourth rule (Keane and Adrian 1990).

Table 3-3: PIV measurement parameters.

Condition	Value
Cardiac cycle duration	0.857 s
dt between laser pulses	200-1000 μs
Frequency of images	340 Hz
Number of images per cycle	294

3.6 *Measurements*

Instantaneous flow rates were measured by one transonic flow meter placed on the tube representing the pulmonary vein. The pressure in the aorta was measured using Millar catheter (Millar Instruments, Houston, Tx, USA, SPC 360S, accuracy 0.5 % full scale). Images capturing

and data evaluation were performed with the software package DaVis 7.2 (LaVision GmbH, Goettingen, Germany).

Time interval between laser pulses (Δt) was optimized for all instants during the cardiac cycle in relation to the maximal velocity, i.e., 200μs < Δt < 1000 μs (Keane and Adrian 1990). The recorded image pairs were analyzed by a standard fast Fourier transform based on the cross-correlation of the initial 64 × 64 pixel interrogation windows with 50 % overlap reduced down to the final 32 × 32 pixel interrogation windows with 50 % overlap.

Table 3-4: PIV parameters used for post processing.

Interrogation Region	***Multi pass cross correlation***
	• ***Initial size*** $\mathbf{64 \times 64}$ • ***Final size*** $\mathbf{32 \times 32}$ • ***50% overlap***

Vorticity

Vorticity is defined as the fluid tendency to rotate or circulate at a certain point. There are several methods to evaluate the vorticity of a flow. It has been shown, however, that the fourth-order compact Richardson extrapolation has the least error among the available schemes, and the highest accuracy for PIV data. For such reasons, it was selected to be used to calculate the vorticity fields from the recorded velocity fields (**Etebari and Vlachos 2005)**. The equation is as follows:

$$\frac{du}{dx_i} = \frac{1}{A_r} \sum_{k=1,2,4,8} A_k \frac{u_{i+k} - u_{i-k}}{2k\Delta x_i}$$

Ar, Ak = constants of extrapolation.

In 2D flow the equation is as follows:

$$\boldsymbol{\omega = \frac{du}{dy} - \frac{\partial v}{\partial x}}$$

x, y = spatial coordinates.

u = velocity across x-axis.

v = velocity across y-axis.

Viscous energy loss

The viscous energy loss due to blood viscosity in the flow is calculated by a MATLAB code using the following equation:

$$EL = \sum_{i,j} \int \frac{1}{2} \mu \left(\frac{\partial u}{\partial j} + \frac{\partial v}{\partial i} \right)^2 dv \quad (i, j = x, y)$$

(Stugaard et al. 2015)

Where:

μ = coefficient of blood viscosity.

u = velocity vector component across x-axis.

v = velocity vector component across y-axis.

x, y = coordinates of the 2D Cartesian coordinates system.

Particle tracking and shear accumulation

Particle tracking was performed by using a code already developed in the lab. The code calculates the shear accumulation according to the following equations:

$$PAS = \sum \tau_i \, dt$$

$$\tau_i = \mu \left(\frac{\partial u}{\partial y} + \frac{\partial v}{\partial x} \right)$$

dt = exposure time of the applied shear.

μ = coefficient of blood viscosity.

x, y = coordinates of the 2D Cartesian coordinates system.

u= velocity vector component across x-axis.

v = velocity vector component across y-axis.

3.7 *Uncertainty Analysis*

Calibration and refractive index estimation

Calibration was made to the system by a calibration target of 0.5 mm accuracy. The calibration target was placed at the same position as the laser sheet which is 1 mm thick and an image was taken, 818.5 pixels corresponded to 50.25 mm, which gives a conversion factor of 16.28 pixel/mm.

To investigate the distortion due to the silicone/water glycerol interface, the same calibration target was placed inside and outside the silicone model (Fig. 3-7). In order to minimize the image distortion, the same liquid was placed inside and outside the ventricle. The error found was approximately 0.6 %.

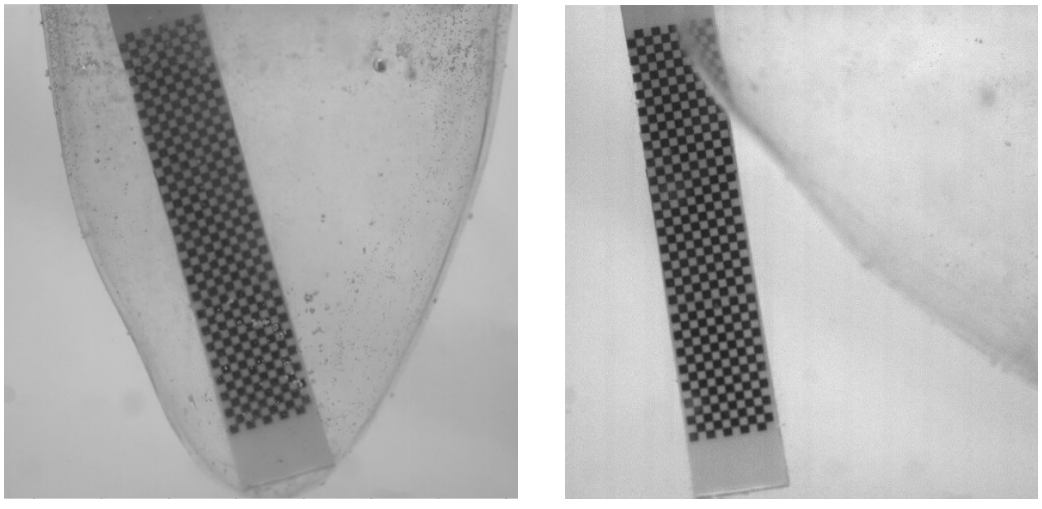

Figure 3-7 Distortion test images inside and outside the left ventricle model.

Uncertainty analysis particle image velocimetry

In this section some parameters that will be used for the errors calculations are defined

Table 3-5: Error calculation parameters (Nishio 2008).

Parameters	Values
Distance of reference point l_r	50.25 mm
Distance of reference image L_r	818.5 pixels
Magnification factor α	0.061 mm/pixel
Distance from the target l_t	0.5 mm

Table 3-6: Error calculations.

Error Name	Description	Equation	Value
Effect of calibration target	The role of the CCD camera is to capture the scattered light from the fluid particles, and the displacement of the particles is estimated using a cross-correlation. The resulting displacement is expressed in pixels and has then to be converted to physical units. For this purpose, a calibration target is used.	Sensitivity= $\partial\alpha/\partial L_r$ = 7.5×10^{-8} m/$pixels^2$. V_{avg} = 0.04 m/s. Error = S × V_{avg}× 0.7 pixels = 0.00003 m/s	= 0.085%

Effect of image distortion at the image edge	The camera optics can cause distortion at the image edge. This error can cause magnification at the image edges.	It was stated that this error does not exceed 0.3% in most experiments (Harris 2012).	= 0.3%
Effect of camera-laser distance	The physical distance between the calibration target and the camera could lead to an error due to a mismatch between the laser sheet and the PIV camera.	Sensitivity= $\partial\alpha/\partial l_t$ = 2×10^{-4} /pixels. Since the laser thickness is about 1 mm, we can assume this difference between the calibration target and the measurement plane is around 0.5 mm Error = $0.5 \times 10^{-3} \times 2\times 10^{-4} \times 651.34 = 6.5\times10^{-5}$.	= 0.162 %
Effect of measurement synchronization	The delay in the trigger can affect the measurements.	It is neglected due to the fact that the recording scale is in seconds while the delay is in	≈ 0%

		nanoseconds, which is negligible.	
Post processing error	The main source of errors is due to mismatching of the two pair of images and subpixel analysis.	dt=1000μs = 0.001s. 1 pixel =0.061mm. V= 0.061 m/s. Error = V × 0.23 = 0.014 m/s.	= 3.5 %

The total uncertainty error analysis due to PIV measurement is approximately 4 %. However, it is important to note that there are other sources of error which are difficult to quantify. Such errors could be found from gradients of velocities, unfocused particle images, poor image quality, and non-homogenous particle image density

CHAPTER 4: RESULTS & DISCUSSION

In this chapter, the results of the experimental recordings are discussed. The comparison in each set between the pathological *vs* the normal case is in terms of velocity fields, viscous energy loss, vorticity fields and histograms, vortex formation time, viscous shear stresses and particle trajectories.

4.1 *Flow Rate & Aortic Pressure*

The experimental setup described in chapter 3 was adjusted to obtain physiological conditions for the aortic pressure and the mitral flow rate at a heart rate of 70 bpm. Both parameters have been measured and recorded for all tested cases. One case is shown in Fig. 4-1 for the flow rate obtained.

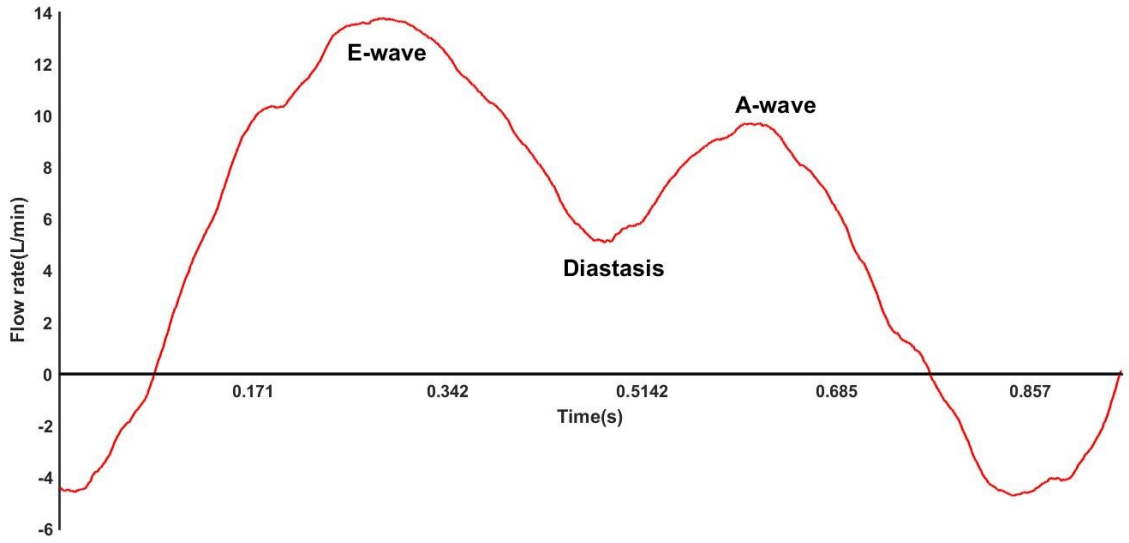

Figure 4-1 Flow rate measured during experiments.

4.2 *In Vitro Experiments*

Table 4-1 shows the tested cases along with their eccentricity values and notation used for this chapter.

Table 4-1: Tested cases eccentricity and notation.

Case	Eccentricity	Notation
Normal	0	N
Mild	0	M
Moderate	0	Mo
Moderate oriented	0.22	MoR
Severe	0	S
Severe oriented 1	0.22	So1
Severe oriented 2	0.44	So2

Velocity fields

Velocity fields were acquired from Lavision Inc. software Davis version 7.1. The mask was chosen as to redraw the inside edge of the ventricle of each post-processed case. Images of specific instant are shown in Fig. 4-2, 4-3, 4-4. The instants chosen are the peak of the E-wave (fast-filling phases), an instant in the diastasis (slow filling phase), and the peak of the A-wave (atrial contraction). These instants were specifically chosen because for a pathology in the left ventricle, the velocity gradients along with other hemodynamics parameters are affected. Throughout different clinical and cardiovascular studies these instants have been chosen to show the effect of cardiac pathologies, hence, allowing clear comparison between different severities. No vectors skipping was applied to the images.

For all cases, the cardiac cycle started with a rapid filling phase (E-wave) characterized by a strong jet entering with velocities in the order of 10^{-1} m/s. The jet was followed by a vortex formation lasting until the diastasis with relatively low velocities (in the order of 10^{-2}). Then, the

A-wave occurred characterized by another strong jet. The velocities of the A-wave are relatively lower than that of the E-wave but both having the same order of magnitude.

Effect of orifice area

Comparing the centered orifices (Fig. 4-2), it is shown that as the severity increases the maximum velocity along with the velocity gradients increase during both the E-wave, diastasis and A-wave (normal up to 1.01 m/s, mild up to 1.54 m/s, moderate up to 2.08 m/s, and severe up to 1.7 m/s). Another observation that can been seen directly in the figures is that as the severities increase, the jet width decreases due to a decrease in the mitral orifice area.

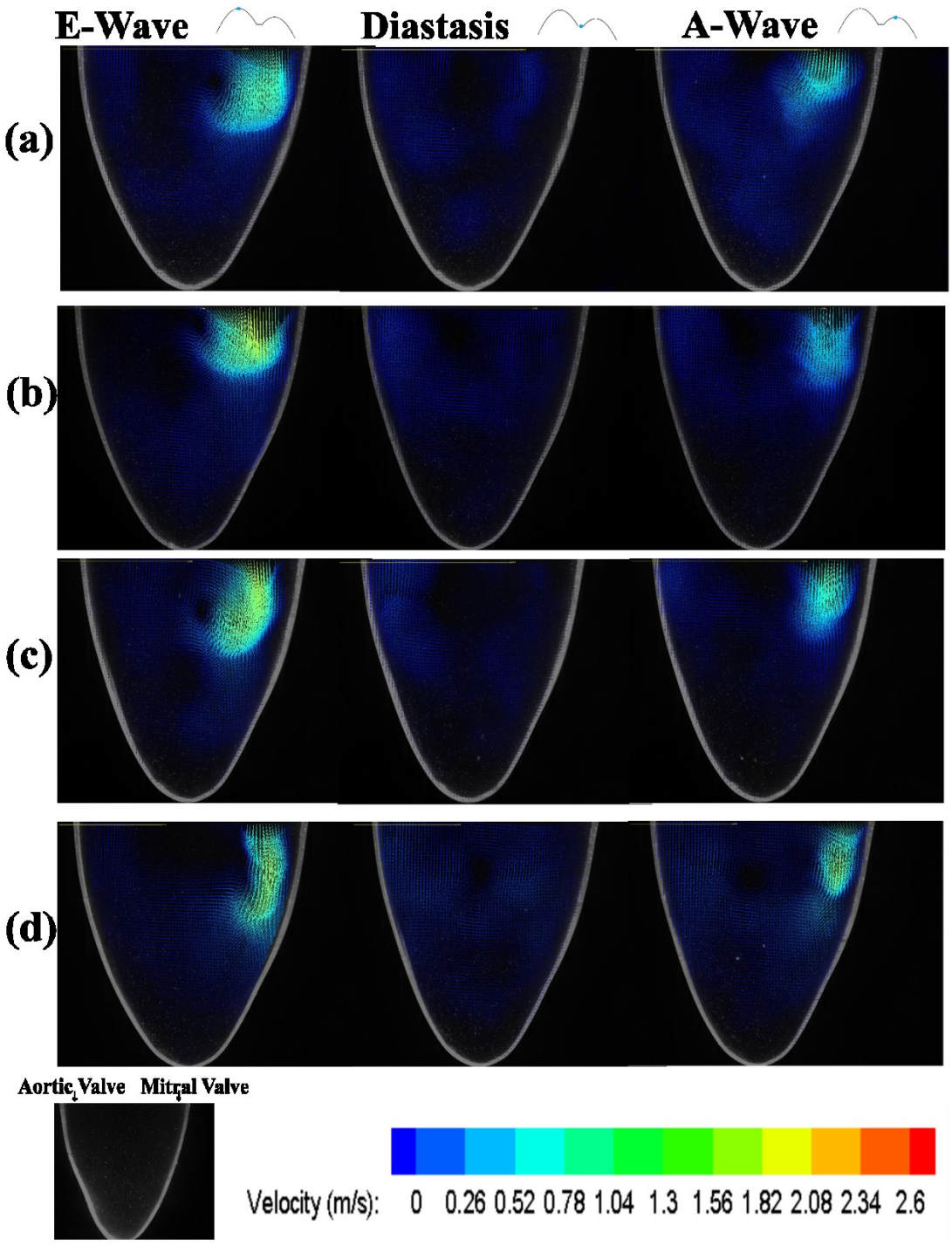

Figure 4-2 Velocity fields for (a) normal, (b) mild, (c) moderate, and (d) severe cases.

Effect of orientation

Fig. 4-3 and 4-4 show a comparison between the moderate cases, and the severe cases, respectively. By this comparison, it is shown that as the orifice eccentricity increases, the

maximum velocity along with the velocity gradients increase markedly throughout the whole cardiac cycle stages (moderate up to 2.08 m/s, MoR up to 2.1 m/s, severe up to 1.7 m/s, So1 up to 1.98 m/s, So2 up to 2.57 m/s).

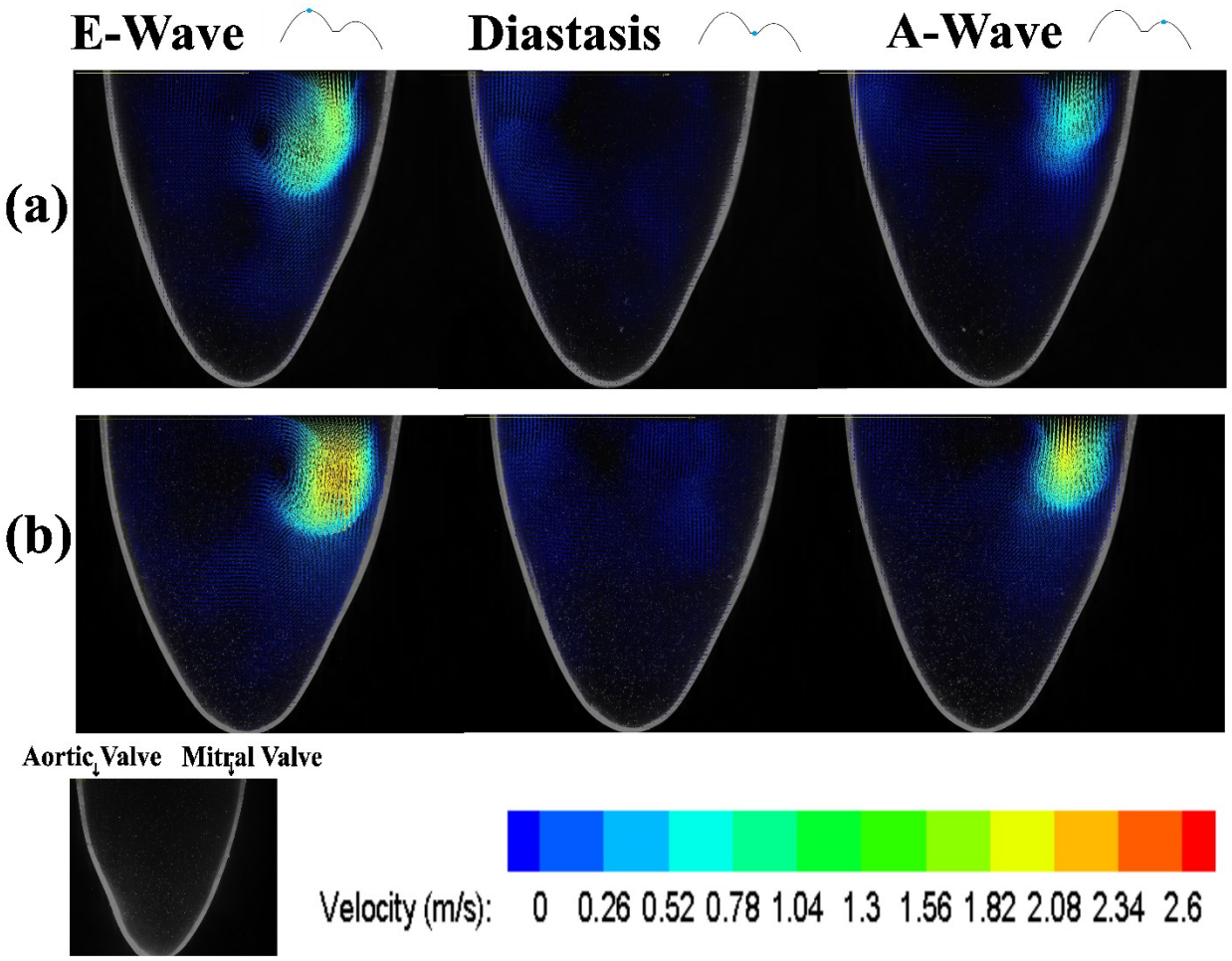

Figure 4-3 Velocity fields for (a) moderate and (b) moderate oriented cases.

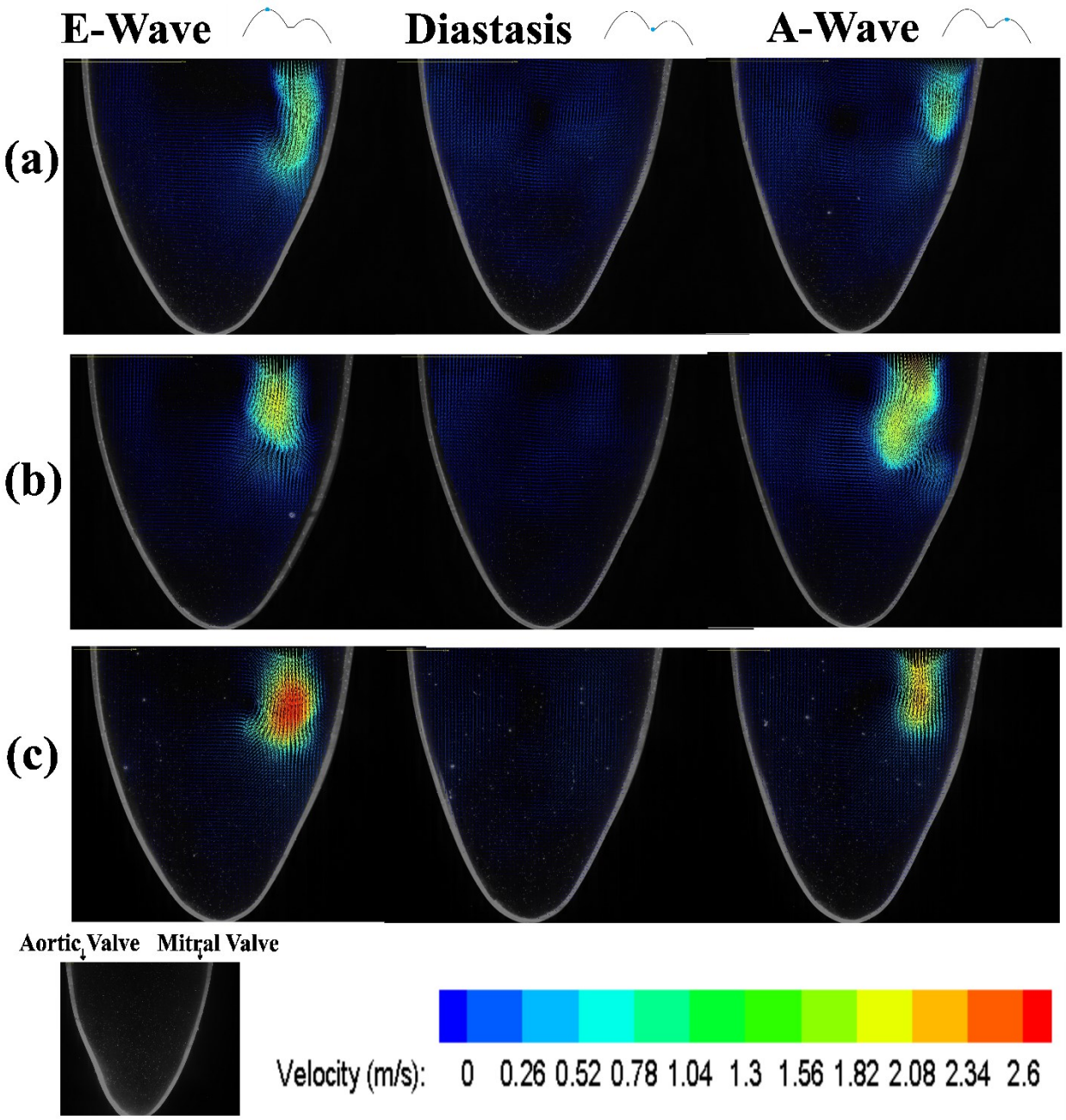

Figure 4-4 Velocity fields for (a) severe, (b) severe oriented 1, and (c) severe oriented 2 cases.

Viscous energy loss

Effect of orifice area

The viscous energy loss in the left ventricle for one cardiac cycle was calculated using a custom made MATLAB code. Viscous energy loss evolution as a function of time curves were plotted.

No filter or smoothing was applied to the curves. In Fig. 4-5, comparing cases with centered mitral valve the energy loss increased as the severity increased. The maximum value for the mild case was 1.17 times that of the normal case, while it was 2.45 and 4.45 times that of the normal case in the moderate, and severe cases respectively.

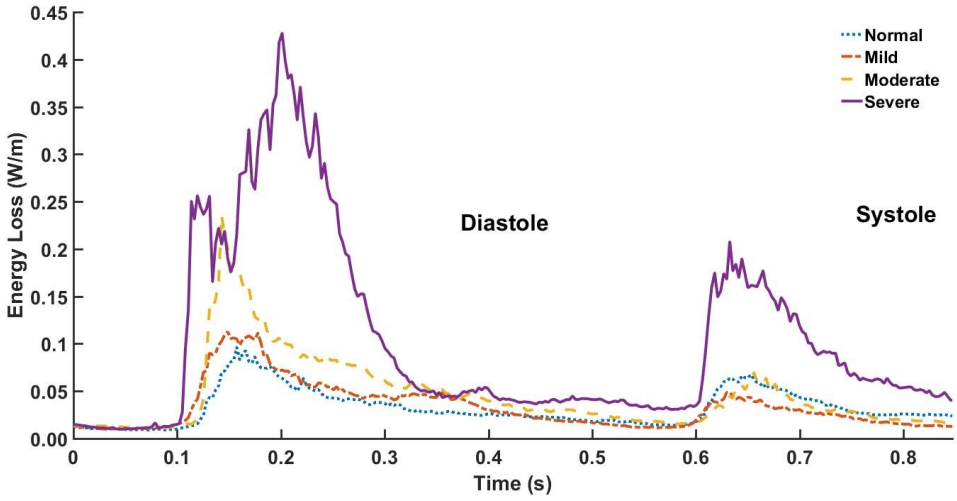

Figure 4-5 Energy loss variation as a function of time for the tested cases.

Comparisons in terms of average values are displayed in Fig. 4-6. This figure shows that MAC induces significant differences in terms of energy losses in the LV ($p < 0.05$) for all cases, except between the normal and mild cases.

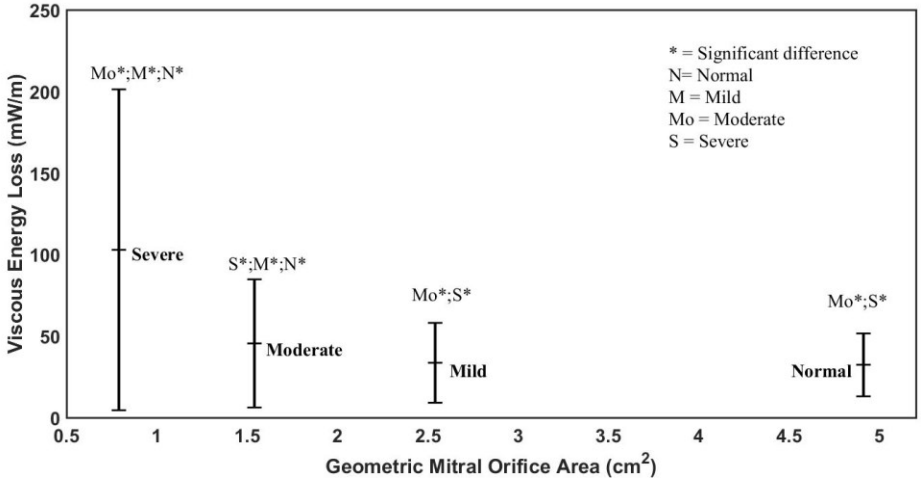

Figure 4-6 Viscous energy loss in the LV as a function of mitral geometrical area

For the moderate cases (Fig. 4-7), the viscous energy loss for the moderate oriented case increased especially during the A-wave, but the maximum energy loss was similar for both cases. The change in jet orientation led to significant differences compared to the normally oriented case ($p < 0.05$) (Fig. 4-8).

Effect of orientation

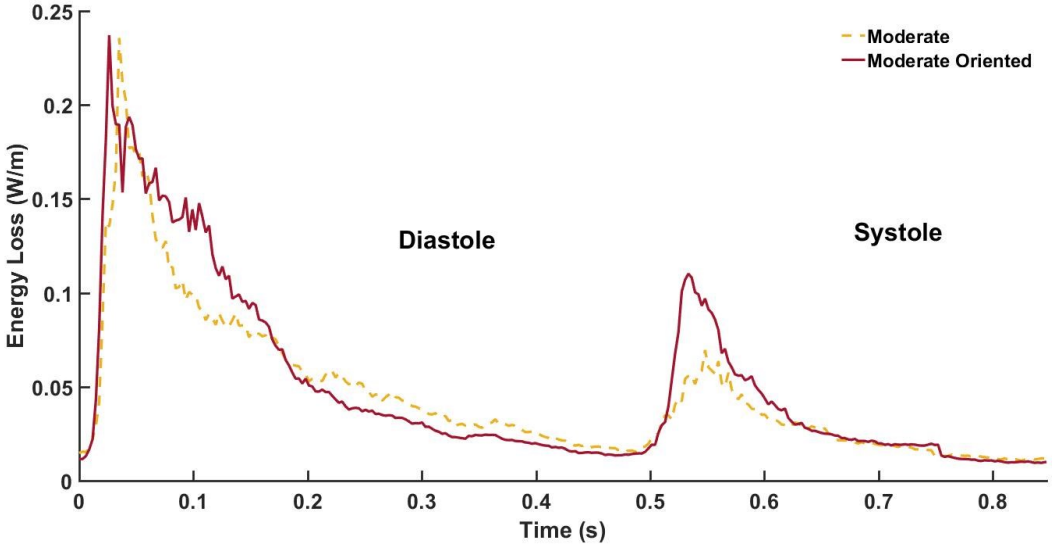

Figure 4-7 Comparison between energy loss variations as a function of time for moderate cases.

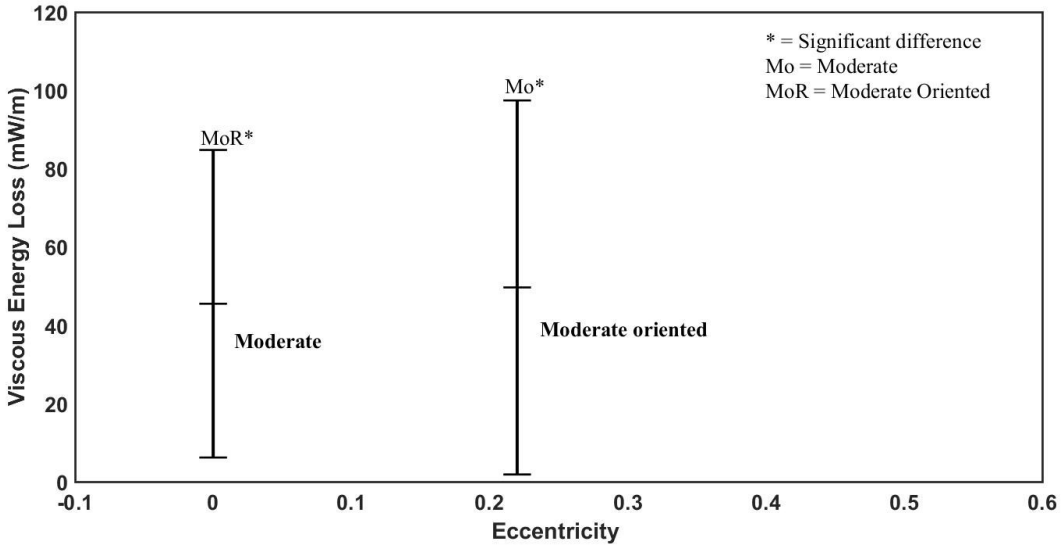

Figure 4-8 Effect of orifice orientation on the energy loss for the moderate case.

As for the severe cases (Fig. 4-9), the energy loss for both the E and the A-wave increased as the eccentricity increased. The curves are significantly different ($p < 0.05$) (Fig. 4-10), and the ratio of the severe oriented 1 and severe oriented 2 over the severe case is 1.41 and 1.73, respectively.

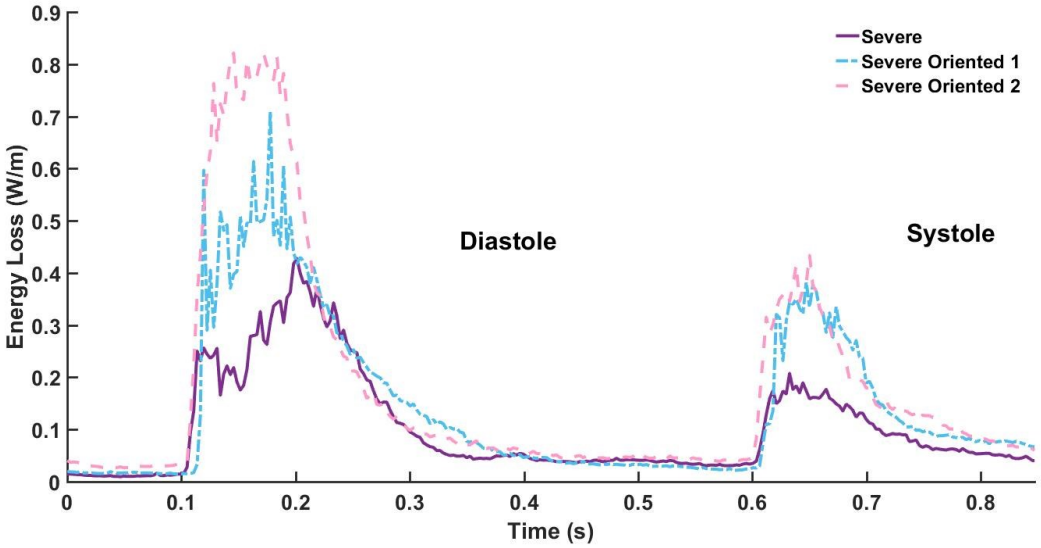

Figure 4-9 Comparison between energy loss variations as a function of time for severe cases.

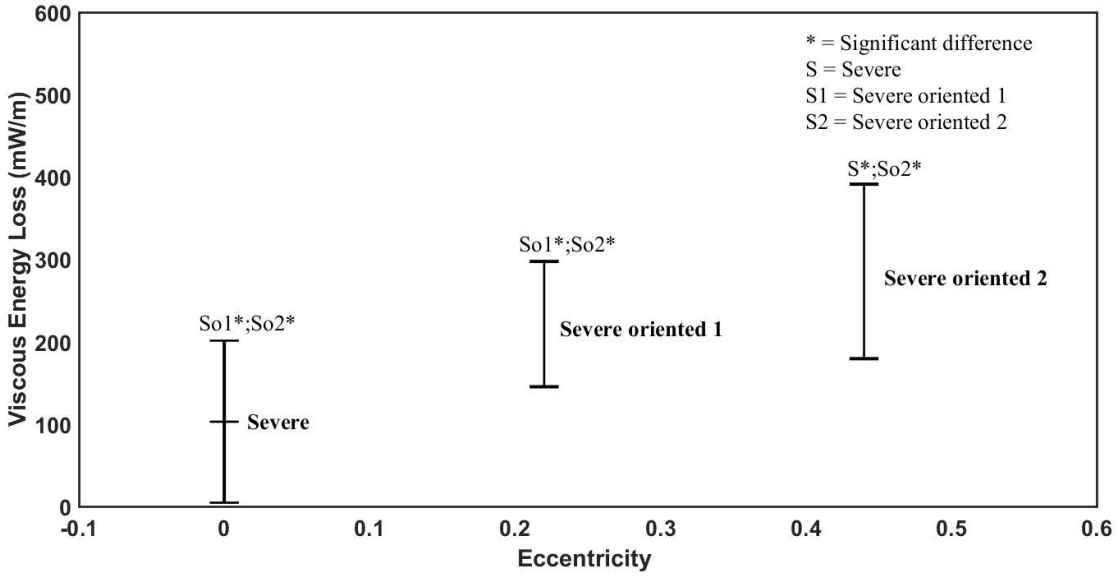

Figure 4-10 Effect of orifice orientation on the energy loss for the severe cases.

Vorticity fields and vorticity histograms

Effect of orifice area

Figure 4-11 shows the vorticity fields for centered cases in three specific instants: the E-wave, diastasis, and A-wave. The flow is characterized by high vorticity gradients with the entering jet in both the E-wave and A-wave, while the vorticity is significantly lower during diastasis. This pattern is repeated in all cases. As for the vorticity magnitudes, the magnitudes increase with the increasing severity. This is clearly shown in Fig. 4-12, where the vorticity histogram range increases with severity (normal ranging from -673.9 to 578.9 /s, mild from -838.6 to 668.6 /s, moderate from -862.2 to 952.2 /s, and severe from -1151 to 1191 /s).

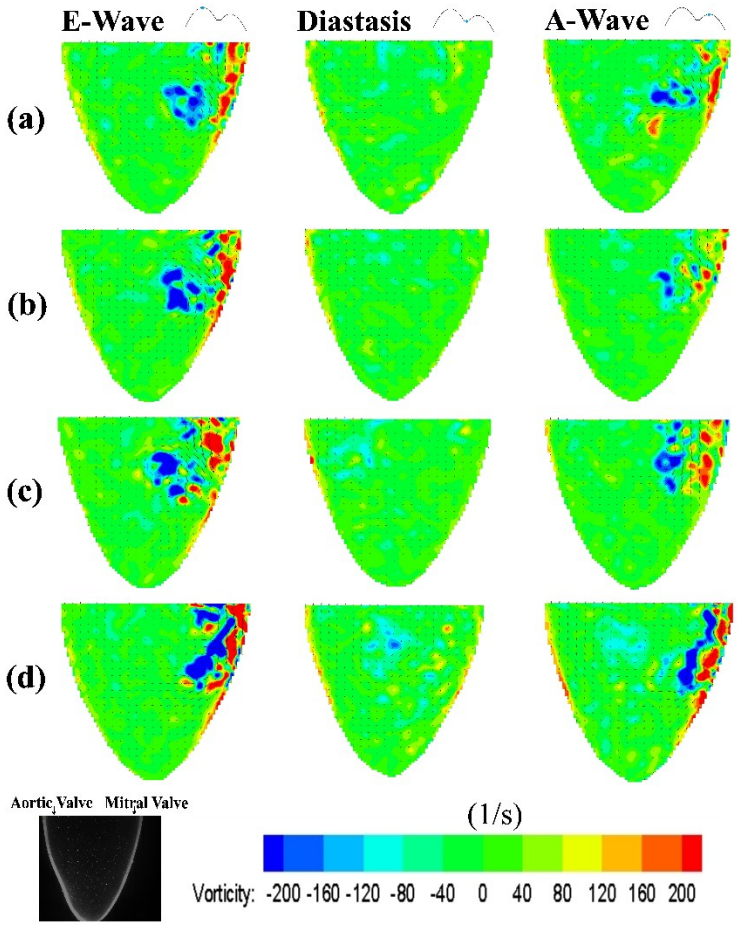

Figure 4-11 Vorticity fields for (a) normal, (b) mild, (c) moderate, and (d) severe cases.

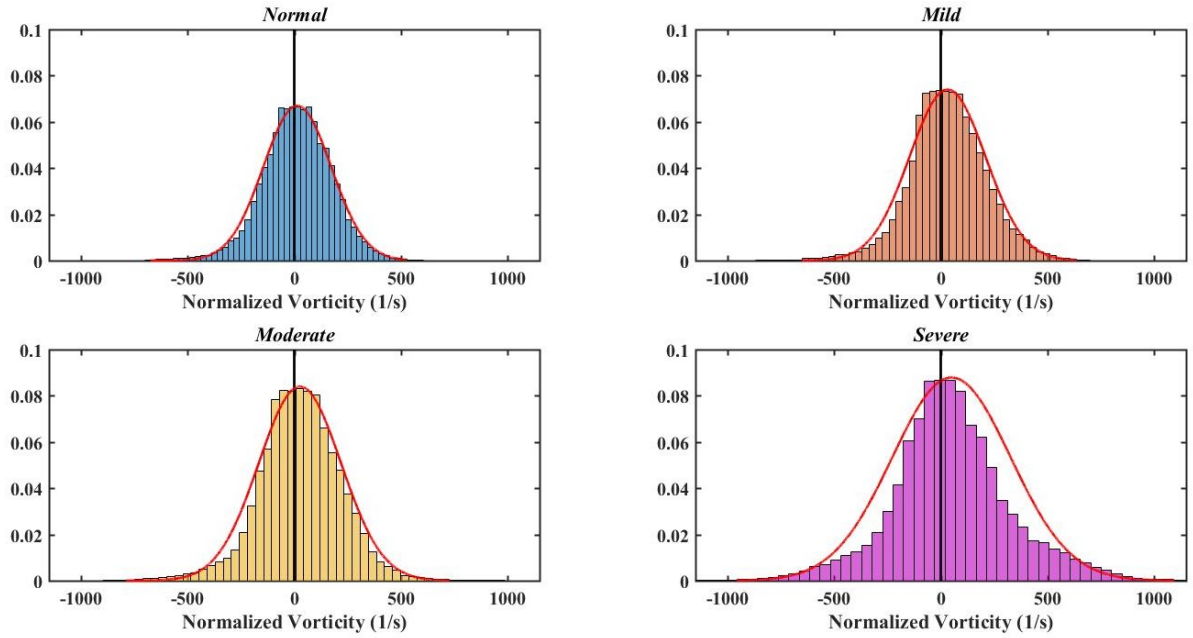

Figure 4-12 Comparison between vorticity histograms for anatomically oriented cases.

Effect of orientation

Now, the vorticity distribution while keeping the same severity but with different orientation is shown in Fig. 4-13 & 4-15. The corresponding histograms are shown in Fig. 4-14 & 4-16. The vorticity histograms of both moderate *vs* moderate oriented, and severe *vs* SO1 *vs* SO2 show that the range of vorticity increases significantly with changing orientation (moderate ranging from -862.2 to 952.2 /s, MoR from -981.8 to 851.8 /s, severe from -1151 to 1191 /s , So1 -1695 to 3345 /s, So2 from -1608 to 1848/s). .

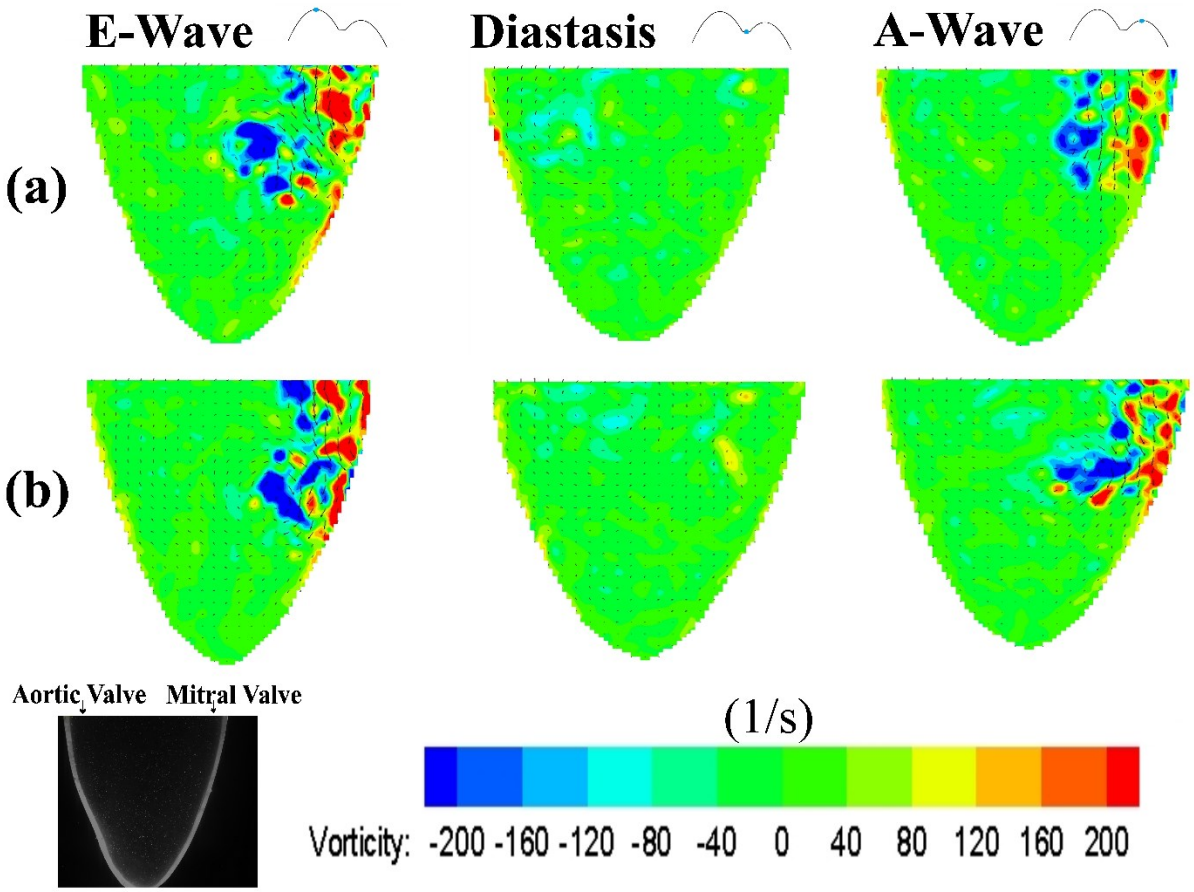

Figure 4-13 Vorticity fields for (a) moderate and (b) moderate oriented cases.

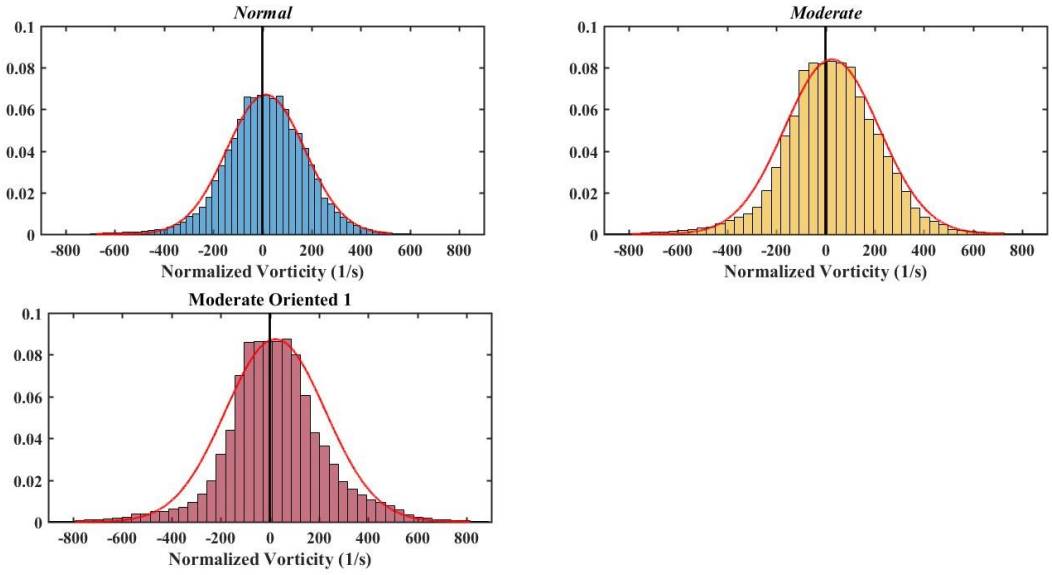

Figure 4-14 - Comparison between vorticity histograms for moderate cases.

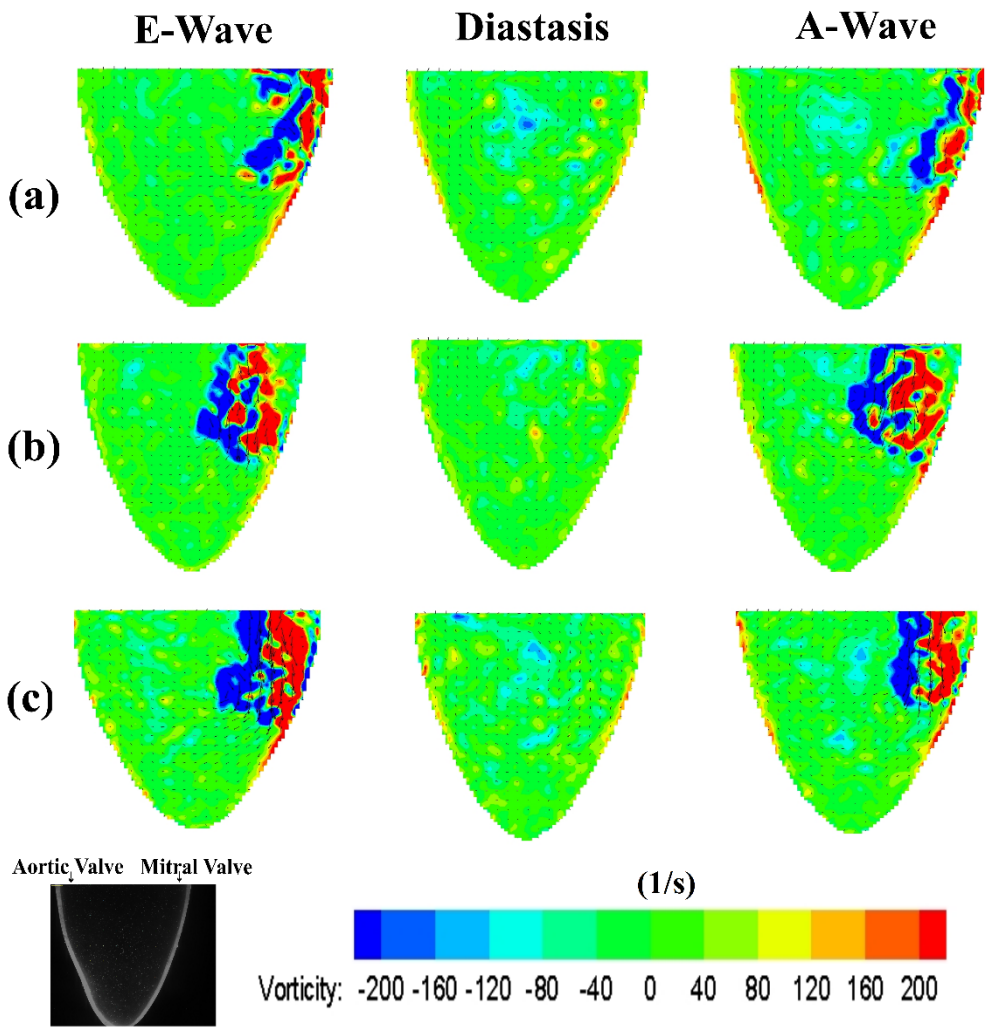

Figure 4-15 Vorticity fields for (a) severe, (b) severe oriented 1, and (c) severe oriented 2 cases.

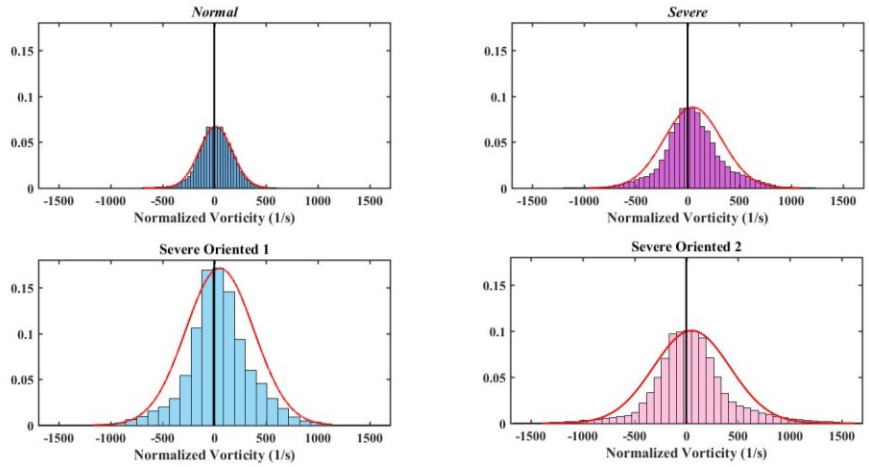

Figure 4-16 Comparison between vorticity histograms for severe cases.

Vortex formation time

The vortex formation time was introduced to characterize vortex rings formed by the fluid ejection from a fixed rigid orifice (Gharib et al. 1998). It is determined as:

$$VFT = \frac{U(t).t}{D}$$

t= ejection duration.

D = orifice diameter.

U(t) = time averaged speed of the fluid flow.

This concept has been applied to the left ventricle E-wave by Gharib et al. (2005), where D is the mitral valve orifice diameter, t is the E-wave duration, and U(t) is the time averaged speed of the mitral inflow (Fig. 4-17). The optimal range for vortex formation time was found as 3.3 < VFT < 5.5 (Gharib et al. 2005) during normal LV function. This range defined the upper and lower limits of VFT and allowed to further evaluate the vortex and the vorticity formed following different cardiac pathologies.

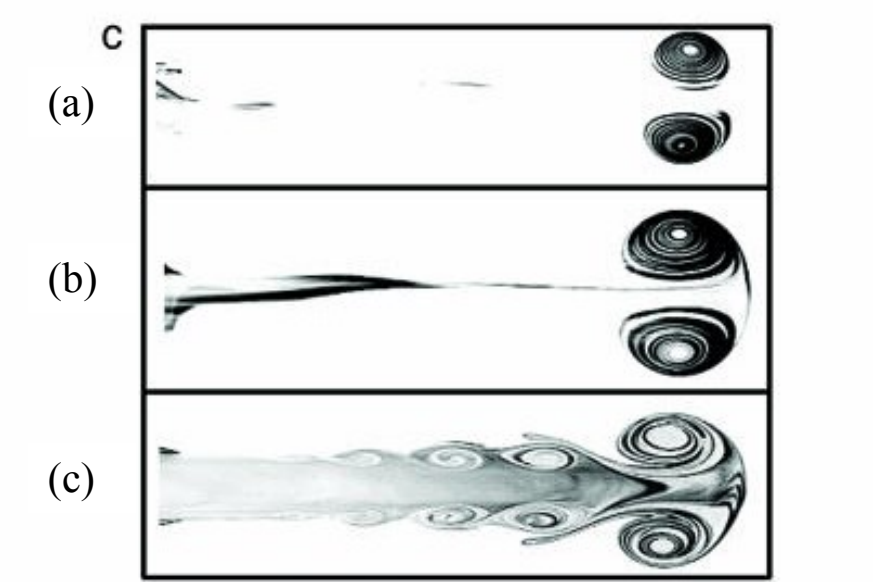

Figure 4-17 Images of in vitro vortex ring with (a) VFT = 2.0, (b) VFT = 3.8, (c) VFT = 14.5

(Gharib et al. 2006)

VFT was calculated for all tested cases and compared to the expected optimal range (Gharib et al. 2006**)** study. A plot showing the VFT for each case along with the optimal range limits is shown in Fig. 4-18.

Effect of orifice area

VFT of the normal case (4.287) is within the optimal range, whereas VFT of mild (7.11), moderate (12.28), and severe case (14.28) were significantly higher than the optimal upper limit (5.5).

Effect of orientation

Both moderate and severe cases VFT exceed the optimal range. However, comparing the moderate (12.28) with moderate oriented (12.85) VFT did not show significant differences, whereas comparing the severe case (14.28) with severe oriented 1 (24.06) and severe oriented 2 (29.02) resulted in a significant increase.

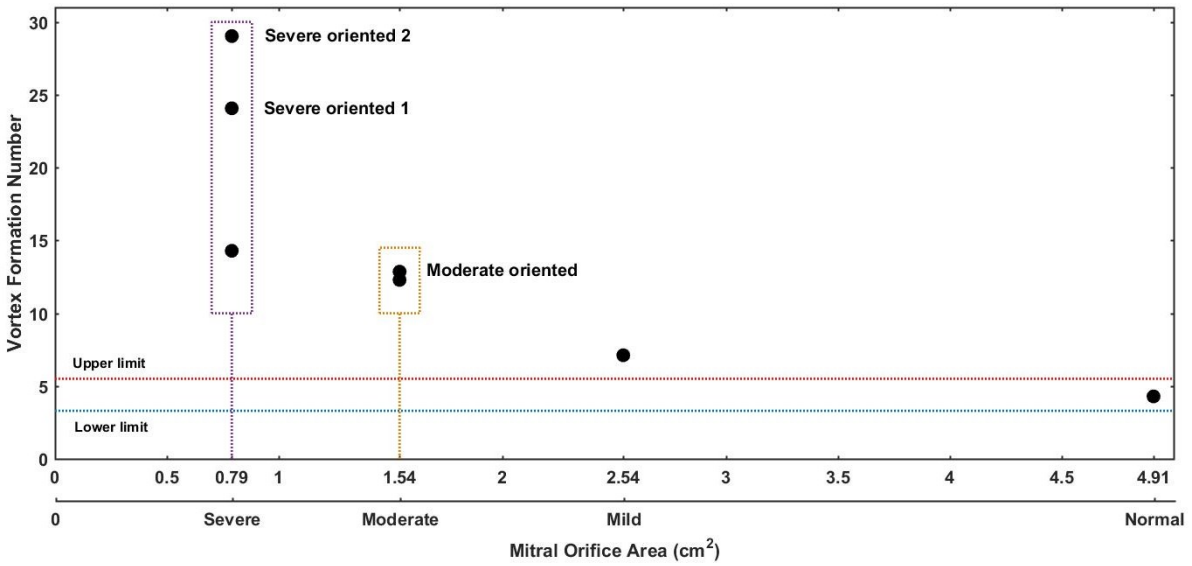

Figure 4-18 Vortex formation time for all tested cases.

For clinical applications, the results regarding VFT have to be taken with caution following the study of Belohlavek in 2012. The authors wrote a paper commenting on the vortex formation time

in terms of limitations. The major limitation mentioned is in the feasibility of obtaining the parameters of VFT in patients, such as mitral diameter. It was suggested that this limitation can be solved by having a four dimensional echocardiographic imaging capable of capturing the required mitral valve data for a one cycle duration.

Viscous shear stress history

Effect of orifice area

Fig. 4-19 shows the viscous shear stress fields for the centered cases in three specific instants E-wave, diastasis, and A-wave. These figures highlight the regions of high shear and regions of low shear. The flow is characterized by high shear stress gradients with the entering jet in both the E-wave and A-wave, while it is significantly lower during diastasis. This pattern is repeated in all cases. As for the shear stress magnitudes, the magnitudes increase with the severity (normal ranging from -2.152 to 2.056 Pa, mild from -2.38 to 3.09 Pa, moderate from -3.1975 to 3.676 Pa, and severe from -4.38 to 4.36 Pa).

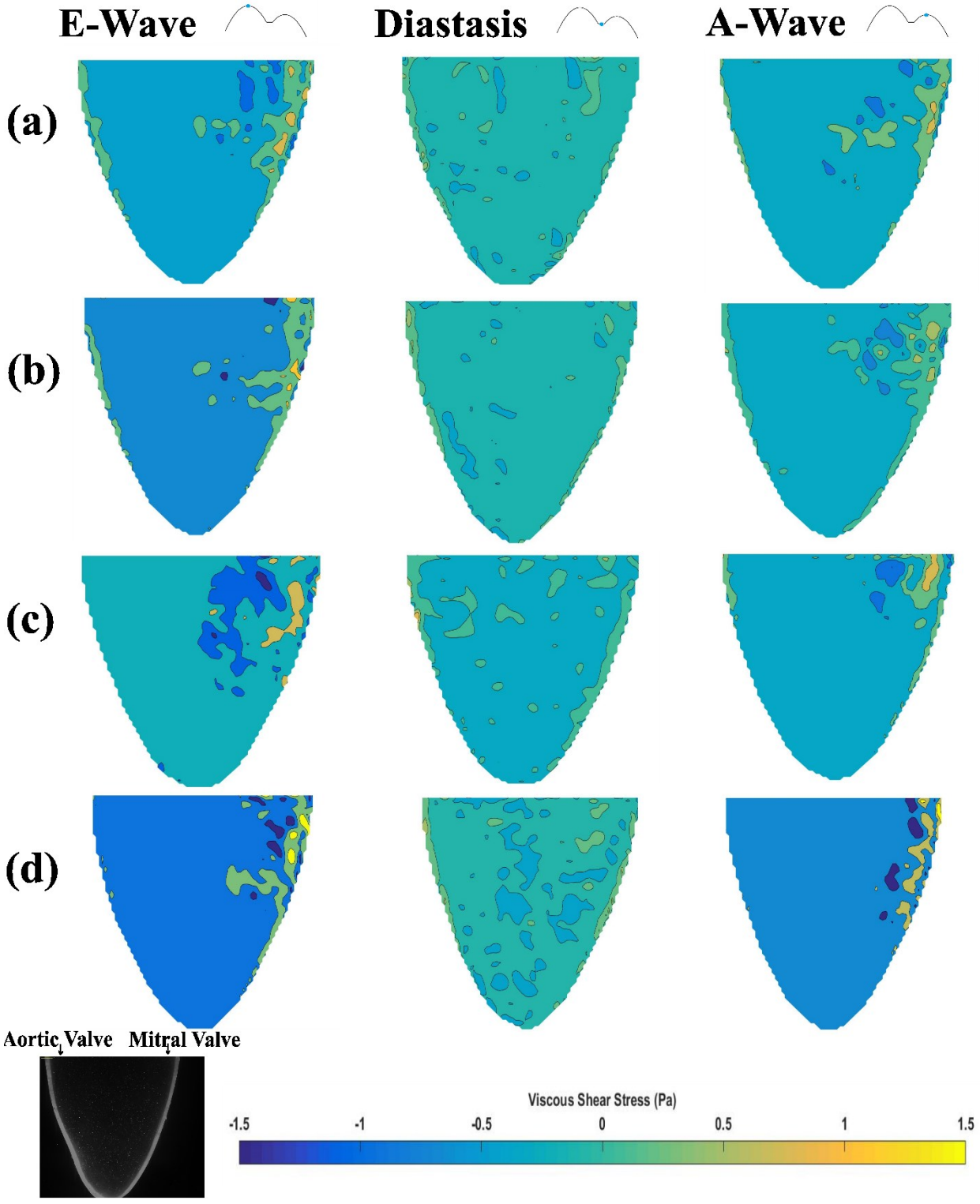

Figure 4-19 Viscous shear stress fields for (a) normal, (b) mild, (c) moderate, and (d) severe cases.

Effect of orientation

Moreover, keeping the same severity but with different orientation is shown in Fig. 4-20 & 4-21. The same flow rate as the centered cases is maintained. Yet, the viscous shear stress gradients increase significantly upon orientation (moderate ranging from -3.1975 to 3.676 Pa, MoR from -3.44 to 3.109 Pa, severe from -4.38 to 4.36 Pa , So1 -12.23 to 5.142 Pa, So2 from –5.67 to 6.562 Pa).

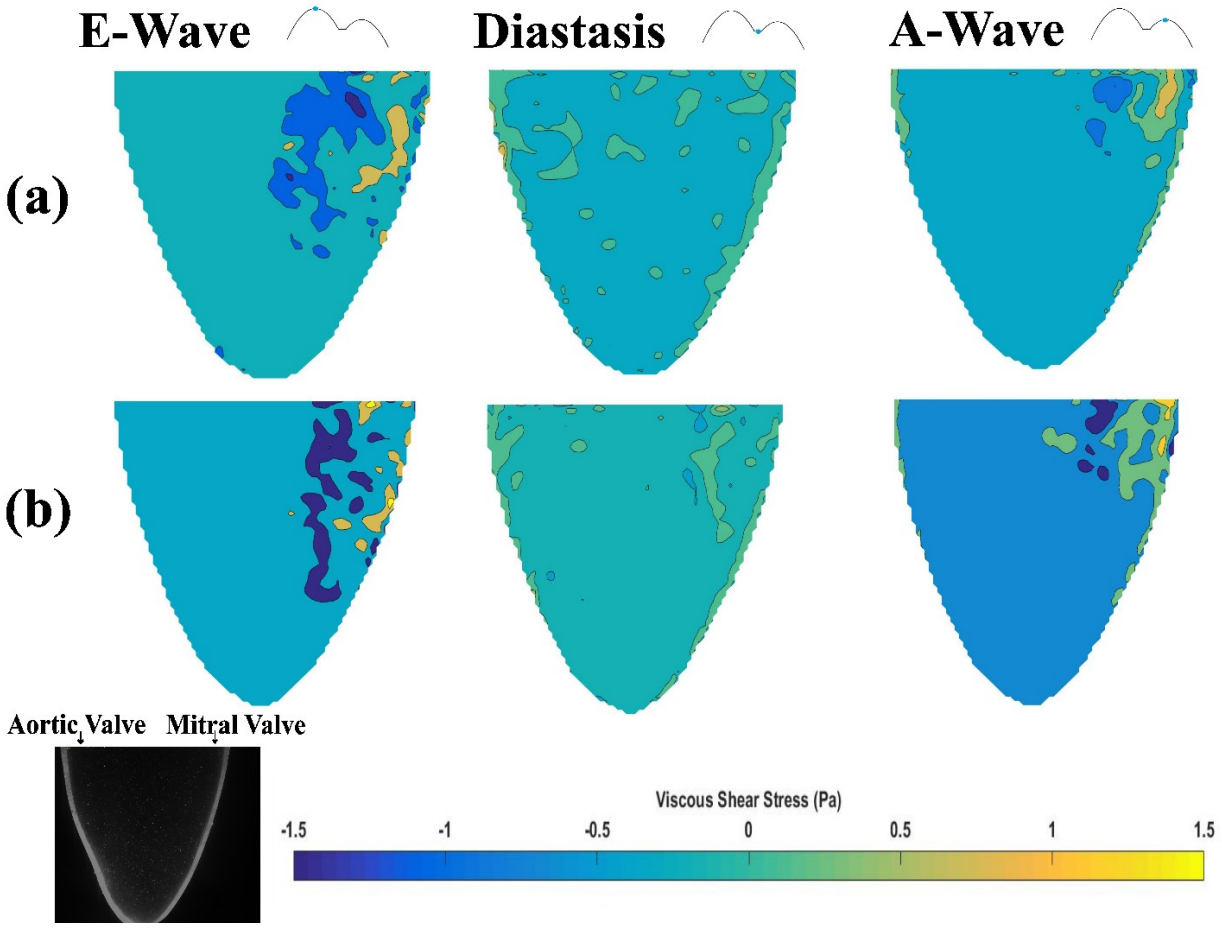

Figure 4-20 Viscous shear stress fields for (a) moderate and (b) moderate oriented cases.

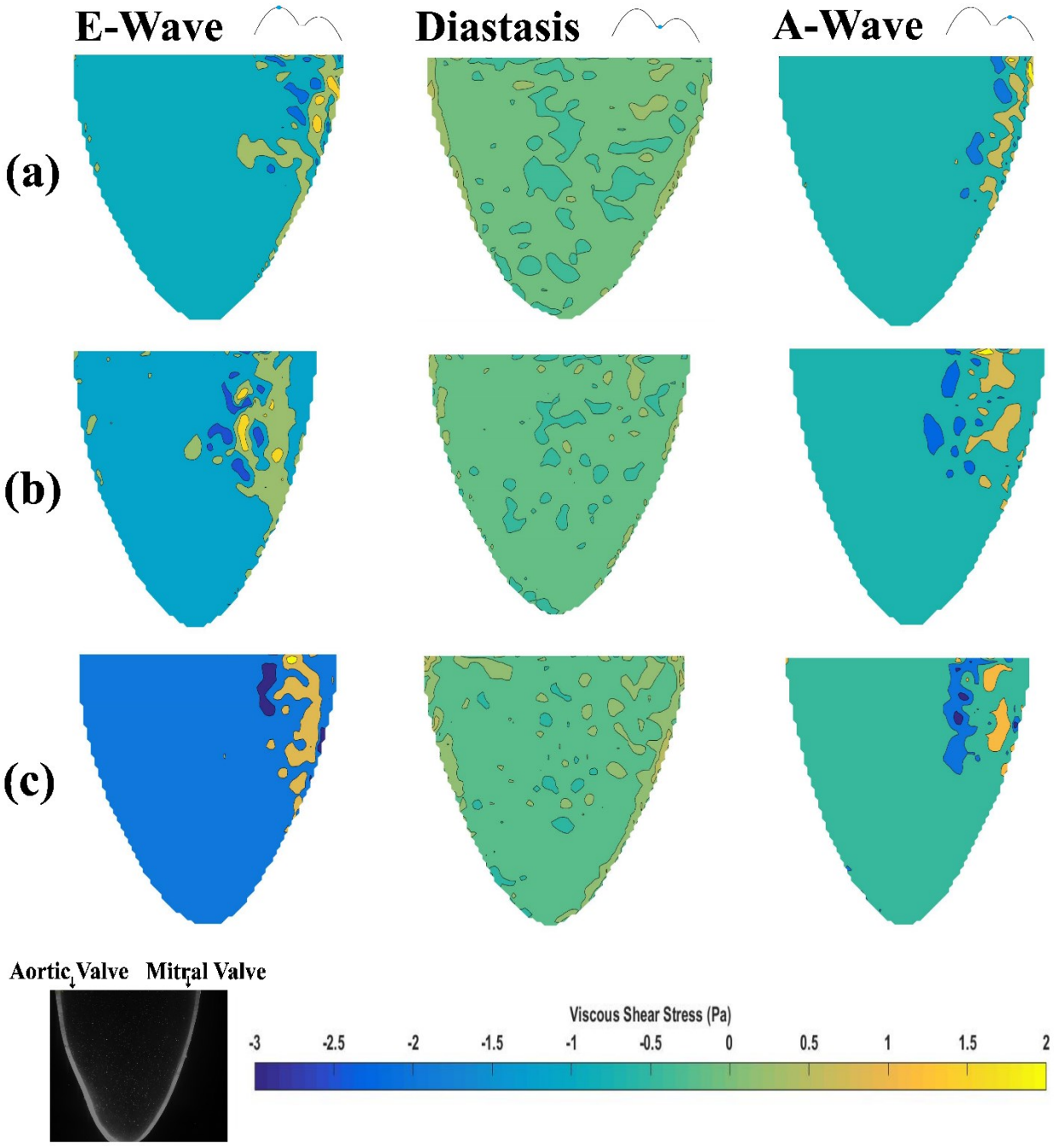

Figure 4-21 Viscous shear stress fields for (a) severe, (b) severe oriented 1, and (c) severe oriented 2 case.

Particle path

A custom made particle path code capable of tracing the particle paths during specified number of cycles, in the ventricle was used.

The code was used to track the particles for one cardiac cycle since the recording was for only a single cycle. Then, eight particle locations were chosen in the ventricle, specifically in the entrance to show the different paths followed by the particles entering the LV.

Effect of orifice area

The different particle paths of the centered orifices cases (Fig. 4-22) show that as the severity increases the path of the particle becomes longer by undergoing looping in some cases. As the path becomes longer, some of the particles which have left in the normal case, remain in the LV in more severe cases.

Effect of orientation

Comparing the particle path of the moderate cases (Fig. 4-23), it is clearly shown that in the moderate oriented case, the path of the particles undergo several loops before leaving. This looping increases the length of the path, affecting shear stresses. Similarly, comparing the severe cases (Fig. 4-24) as the eccentricity increases the path loops becoming longer and less optimized compared to the normal case.

.

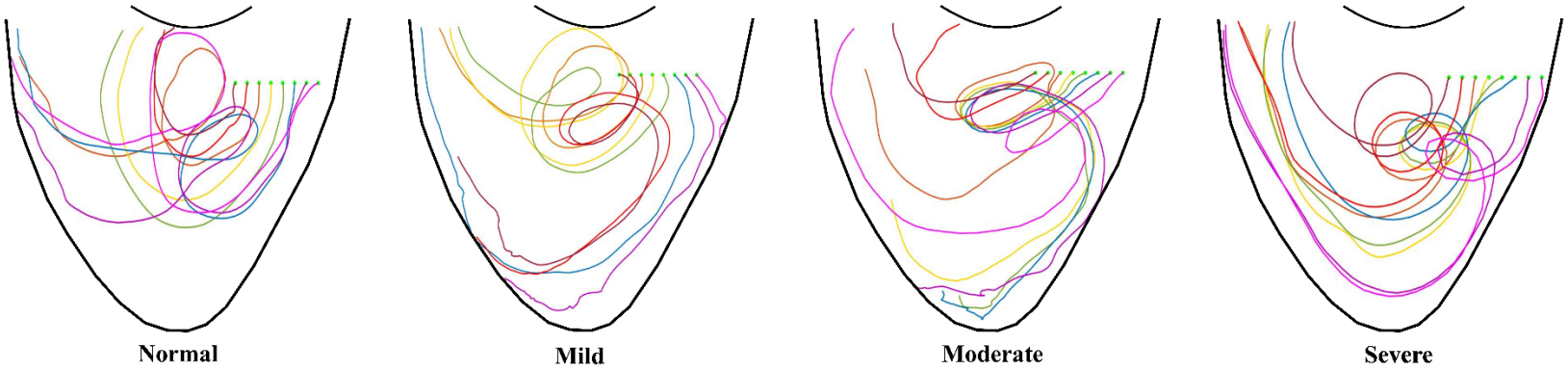

Figure 4-22 Comparison between particle path trajectories in anatomical oriented cases.

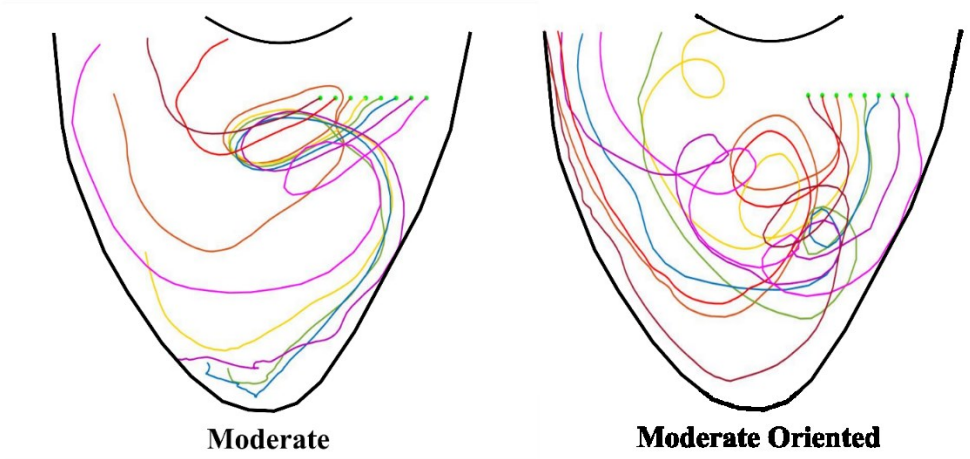

Figure 4-23 Comparison between particle path trajectories in moderate cases.

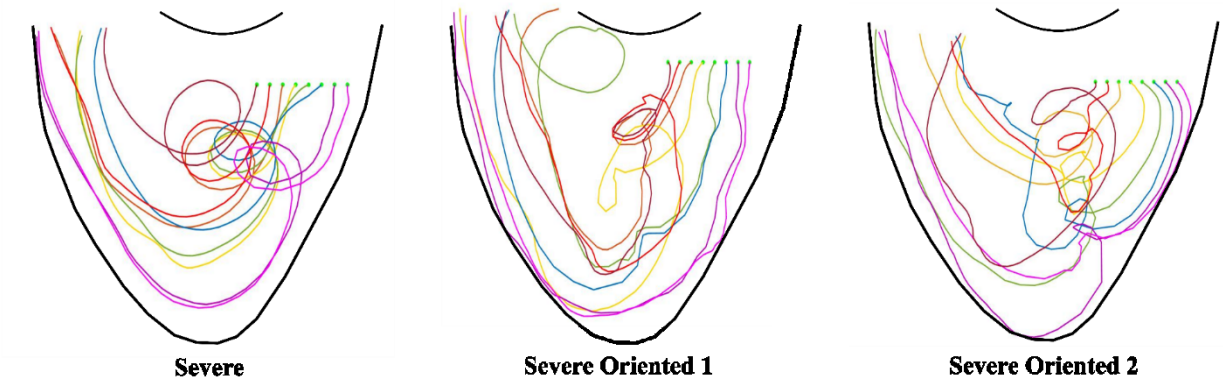

Figure 4-24 Comparison between particle path trajectories in severe cases.

Shear accumulation

For one cardiac cycle, the shear accumulation history was calculated for the same eight particles demonstrated in the particle path section above (Fig. 4-25, 4-26 & 4-27). For each case, eight curves are plotted for the shear accumulation history as a function of time.

Effect of orifice area

For the normal case the pattern is almost linear with a maximum shear accumulation value of 0.089 Pa.s. The mild case deforms from the normal pattern and is like a transitional stage between the normal and moderate. The maximum shear history for the mild, moderate and severe is 0.212, 0.134 and 0.087 Pa.s respectively.

Effect of orientation

Comapring the moderate 0.134 Pa.s with the moderate oriented maximum shear accumulation 0.15 Pa.s shows an increase which can been seen in Fig. 4-27. As for the severe case the maximum shear accumulation for the severe, severe oriented 1, and severe oriented 2 is 0.087, 0.22, and 0.2 respectively. The increase is significantly high in the severe oriented case.

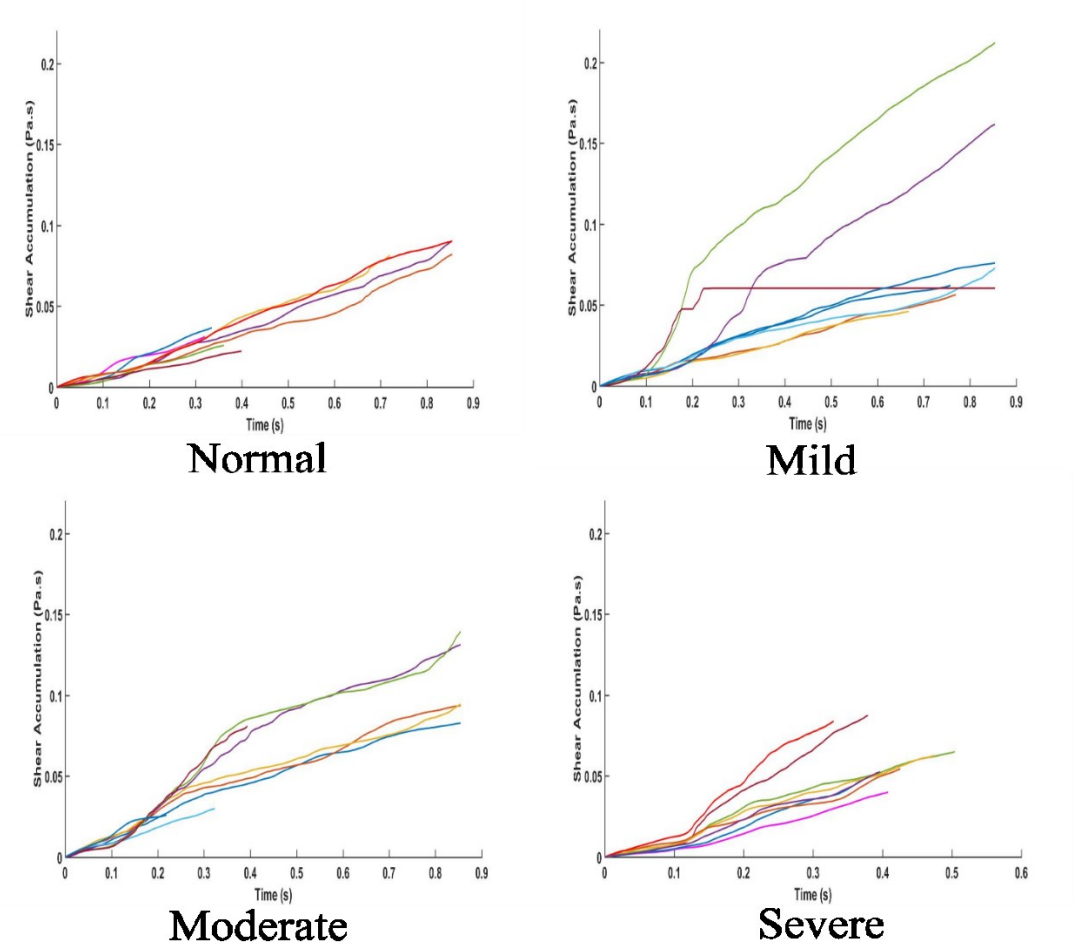

Figure 4-25 Shear accumulation history for centered orifices.

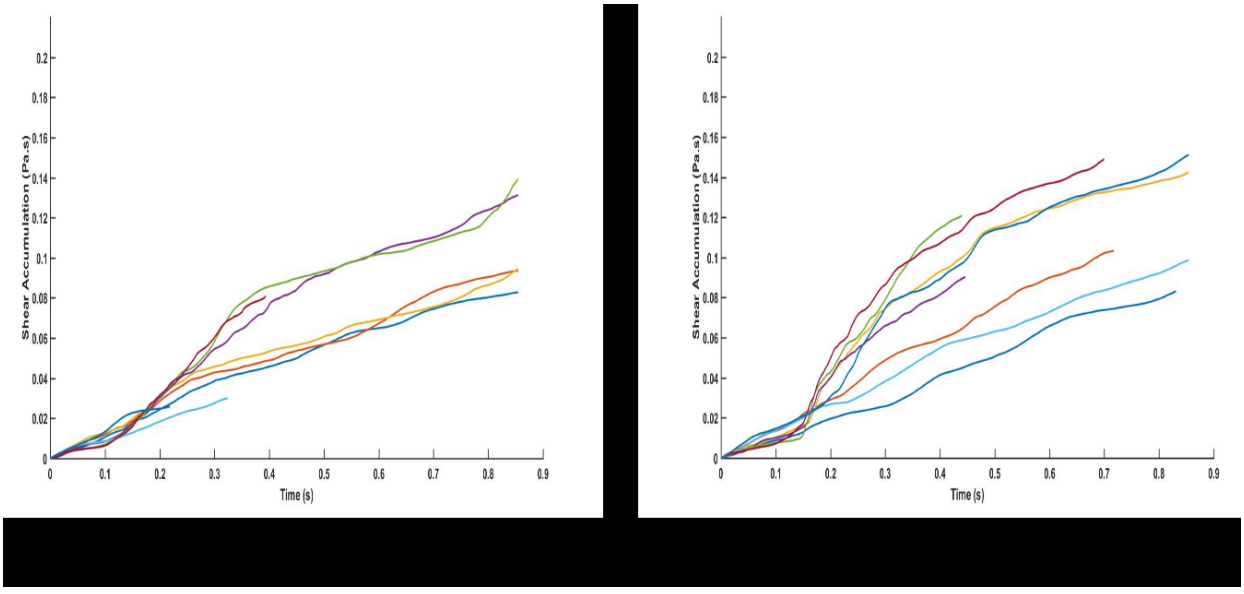

Figure 4-26 Shear accumulation history for moderate cases.

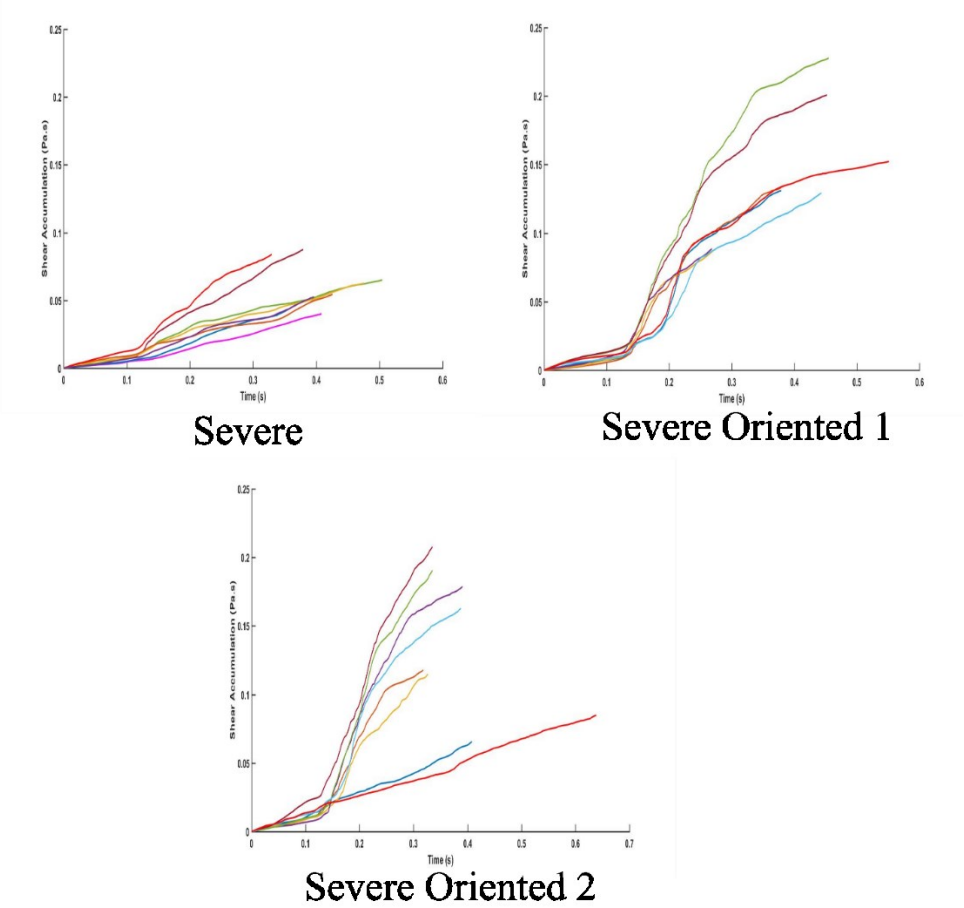

Figure 4-27 Shear accumulation history for severe case.

Fig. 4-29 shows a sketch of the shear accumulation as a function of time for the centered orifices.

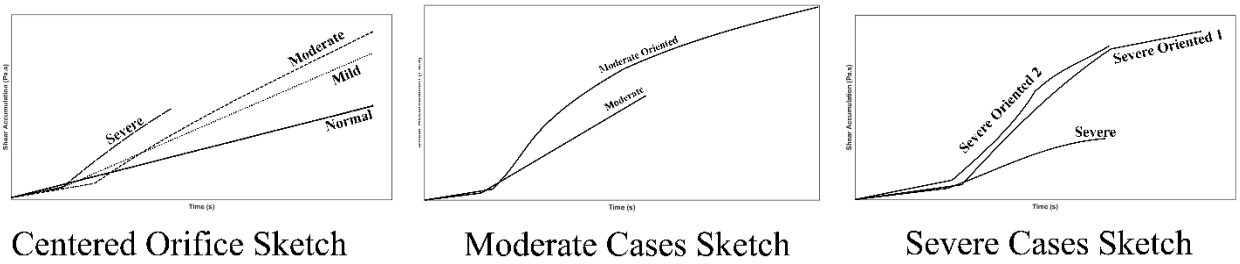

Figure 4-28 Shear accumulation history sketch.

4.3 *Patient Specific Experiments*

Velocity fields

Fig. 4-29 shows the velocity fields for the patient specific cases: normal, moderate and severe at different instants of the cardiac cycle (E-wave, diastasis and A-Wave). In the normal case, the flow is characterized by a strong jet in the E and A-wave, with a diastasis in-between having relatively low velocity magnitudes. The scenario is the same for all three cases.

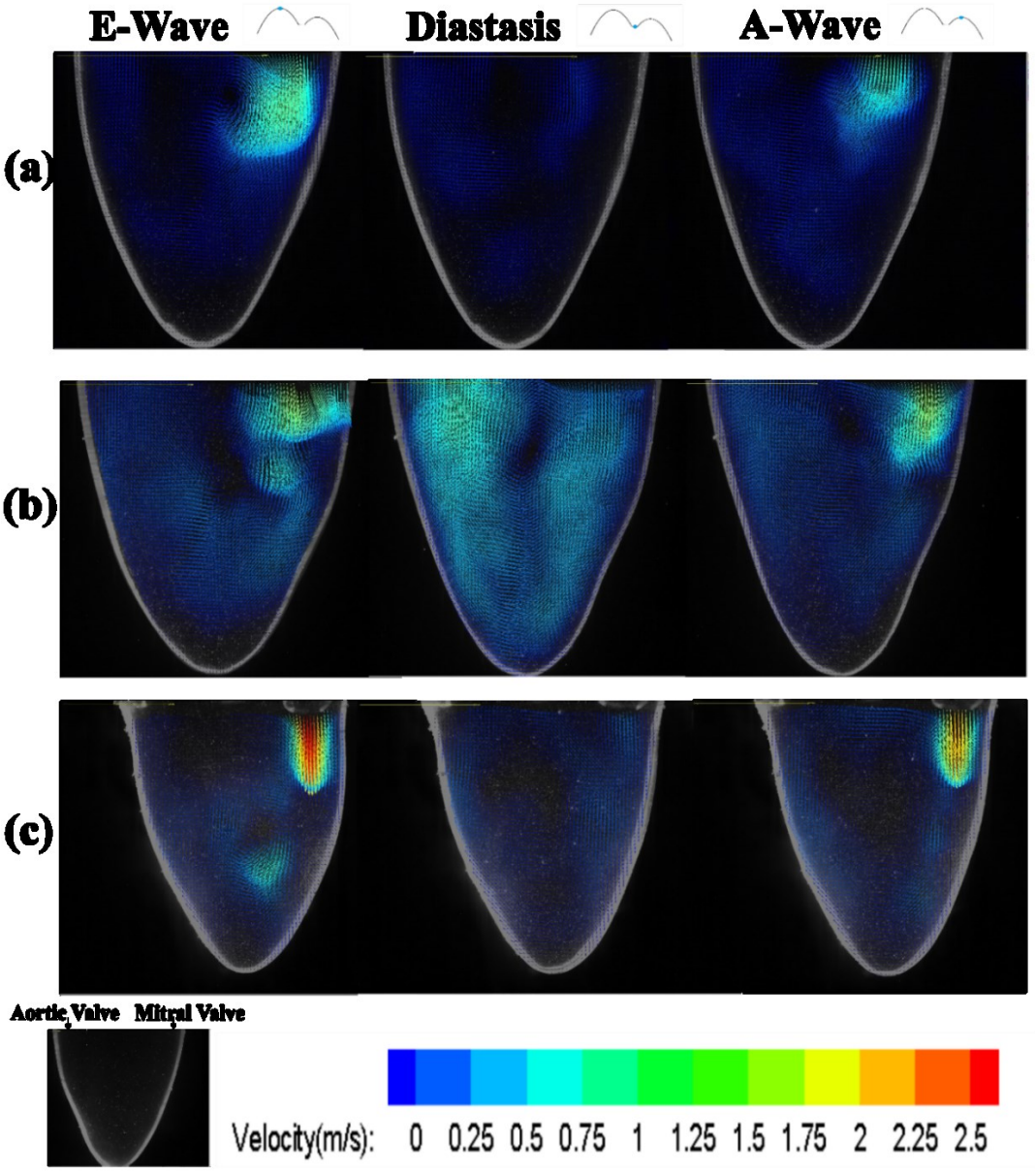

Figure 4-29 Velocity fields for (a) Normal, (b) Moderate and (c) Severe MAC cases.

The maximum velocities for the three cases at specific instants are shown in Table 4-2.

Table 4-2: Maximum velocity for tested cases.

	Normal	***Moderate MAC***	***Severe MAC***
E-wave velocity (m/s)	***1.15***	***1.52***	***2.44***
Diastasis velocity (m/s)	***0.38***	***1***	***0.42***
A-wave velocity (m/s)	***0.94***	***1.43***	***1.92***

The velocity gradients were the highest in the severe case as shown in Fig. 4-29. The highest velocity of the E-wave and the A-wave was in the severe case. The diastasis was different, where the highest velocity was in that of the moderate case, and the lowest was in that of the normal case.

The maximum velocities of the E-wave and A-wave increased as a function of the severities which corresponds well with the study of Soeki et al.2001 on patients with MAC. The study shows that as the severity increases (normal < mild < severe), the E and A velocities increase.

Viscous energy loss

The energy loss due to the blood viscosity in the flow is calculated in the Left Ventricle for one cardiac cycle and compared between different MAC cases. No smoothing or filtering is applied to the curves. The energy loss of the normal case is compared with references found in literature, and correlated well (Akiyama et al. 2017).

The energy loss maximum in the normal case is 0.1837 W/m, while it is 0.4627 W/m in the moderate case and 0.2157 W/m in the severe case (Fig. 4-30). The mean of the normal case graph of energy loss evolution is 0.032 ± 0.019 W/m, which increases for the moderate case 0.12 ± 0.096 W/m and decreases for the severe case 0.031 ± 0.032 W/m (Fig. 4-31).

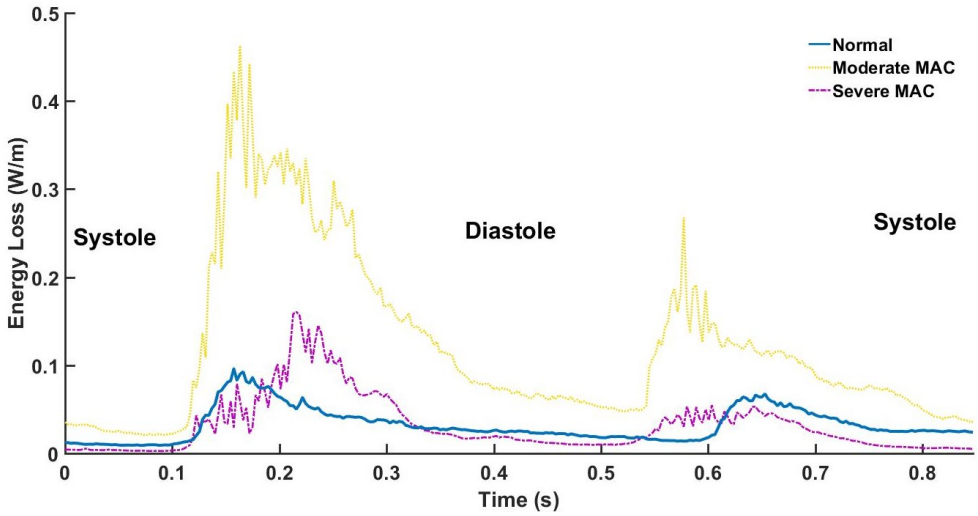

Figure 4-30 Comparison between energy loss variations as a function of time for (a) normal, (b) moderate and (c) severe MAC cases.

Further statistical analysis was applied to the data to extract the curves characteristics. Performing a student t-test to the curves showed significant differences between the normal curve and that of the moderate and severe curves respectively ($p < 0.05$). In addition, comparing the moderate curve with the severe curve gave also significant difference ($p < 0.05$).

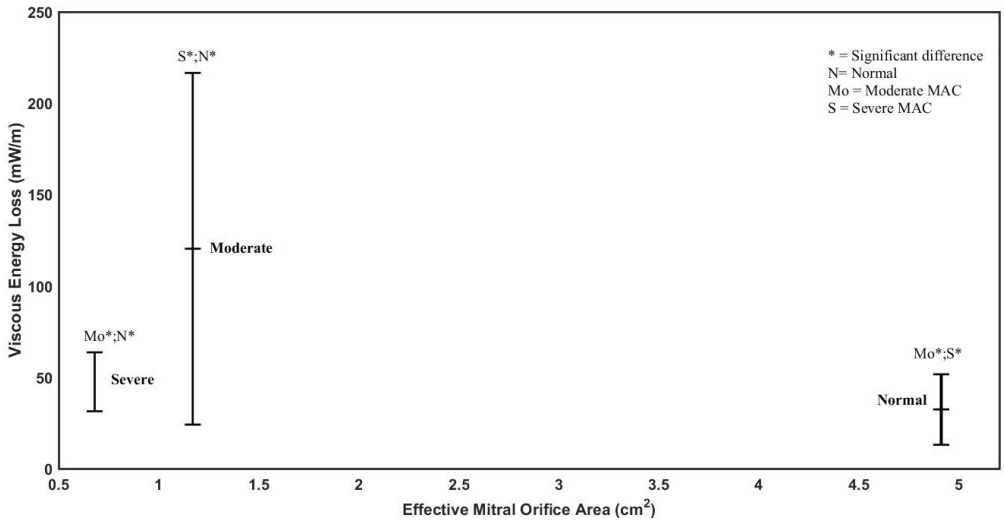

Figure 4-31 Statistical analysis data of the viscous energy loss for (a) Normal, (b) Moderate and (c) Severe MAC cases.

Vorticity fields and vorticity histogram

Instantaneous vorticity values were computed. A figure for each of the three instants is shown for all cases (Fig. 4-31). For all cases, the cardiac cycle starting with the E-wave, is characterized with a strong jet as shown previously with the velocity fields section. This strong jet corresponds to significantly high vorticity values in the location of the jet. Then the vorticity decreases significantly during the diastasis phase. And lastly, it re-increases during the A-wave.

The vorticity histograms give an idea of the vorticity value distributions (Fig. 4-32). The normal case distribution is the closest to a Gaussian curve. The histogram for the moderate case is flatter than that of the normal case and of a wider vorticity range, having fewer small values (close to zero) and more distribution over the higher vorticity values. The severe histogram range is greater than that of the normal case and less than that of the moderate case.

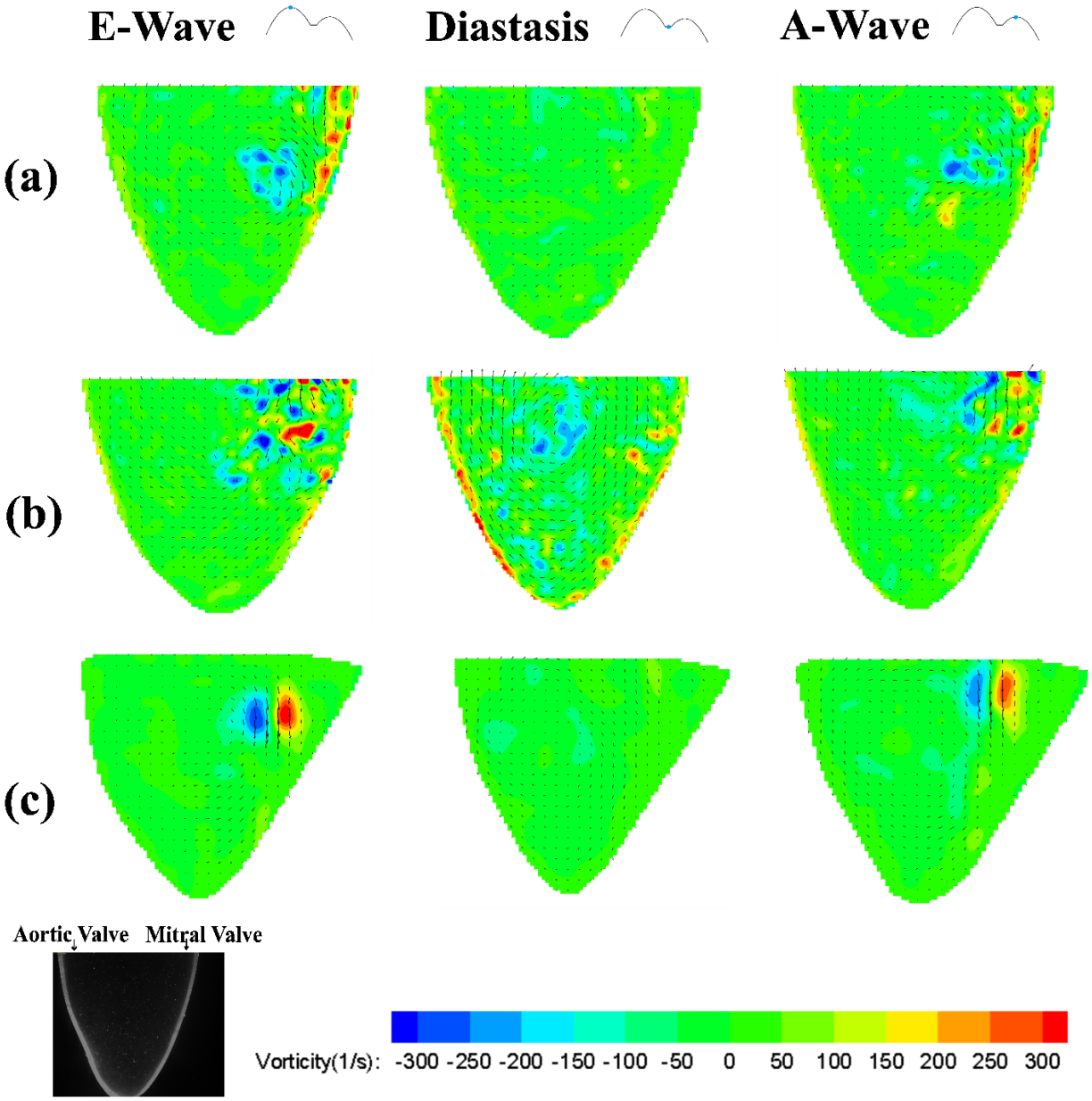

Figure 4-32 Vorticity fields for (a) Normal, (b) Moderate and (c) Severe MAC cases in 1/s.

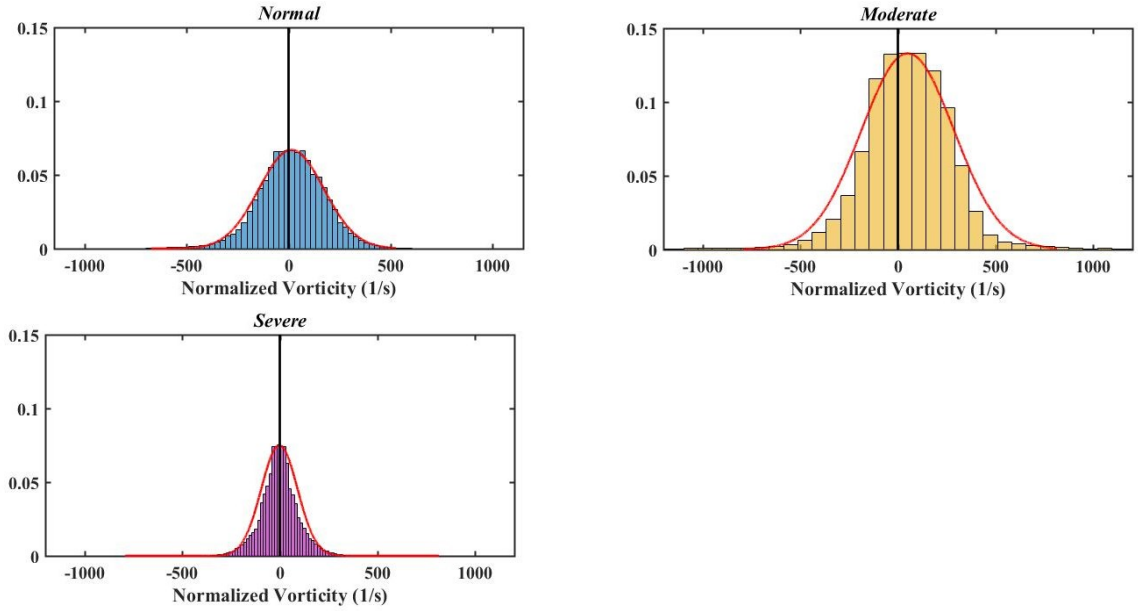

Figure 4-33 Comparison between vorticity histograms for (a) Normal, (b) Moderate and (c) Severe MAC cases.

Vortex formation time

For the calculation of VFT, and as it required the mitral annular diameter for the MAC cases, we decided to use the geometric orifice area of the valve

A figure representing each case with its corresponding VFT, along with the optimal range is plotted (Fig. 4-34). Both moderate (16.77) and severe (37.01) cases VFT exceeded that of the optimal range ($3.3 < VFT < 5.5$), whereas the normal case was within the range ($3.3 < 4.287 < 5.5$). Comparing the moderate and severe with the normal VFT gave a difference of 11.86, and 32.1, respectively. Thus, VFT increases with the increase of the severity of MAC.

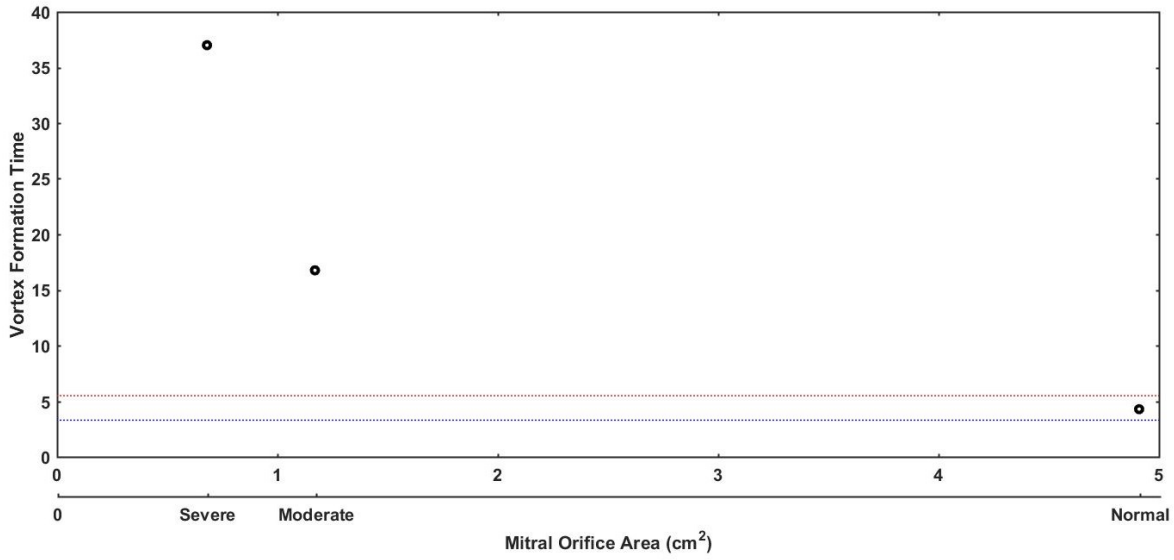

Figure 4-34 Vortex formation time for (a) Normal, (b) Moderate and (c) Severe MAC cases

Viscous shear stress

Instantaneous viscous shear stress values were computed for one cardiac cycle. A figure for each of the three specific instants is shown for all cases (Fig. 4-35). For all cases, the cardiac cycle started with the E-wave, which is characterized with a strong jet and increased vorticity as shown previously. This causes high shear stress values. Then the VSS decreases significantly during the diastasis phase. And lastly, it re-increases during the A-wave.

The viscous shear stress increases for the moderate MAC and severe MAC cases in the E-wave, diastasis and A-wave. Implying that upon the presence of MAC higher shear stresses are imparted.

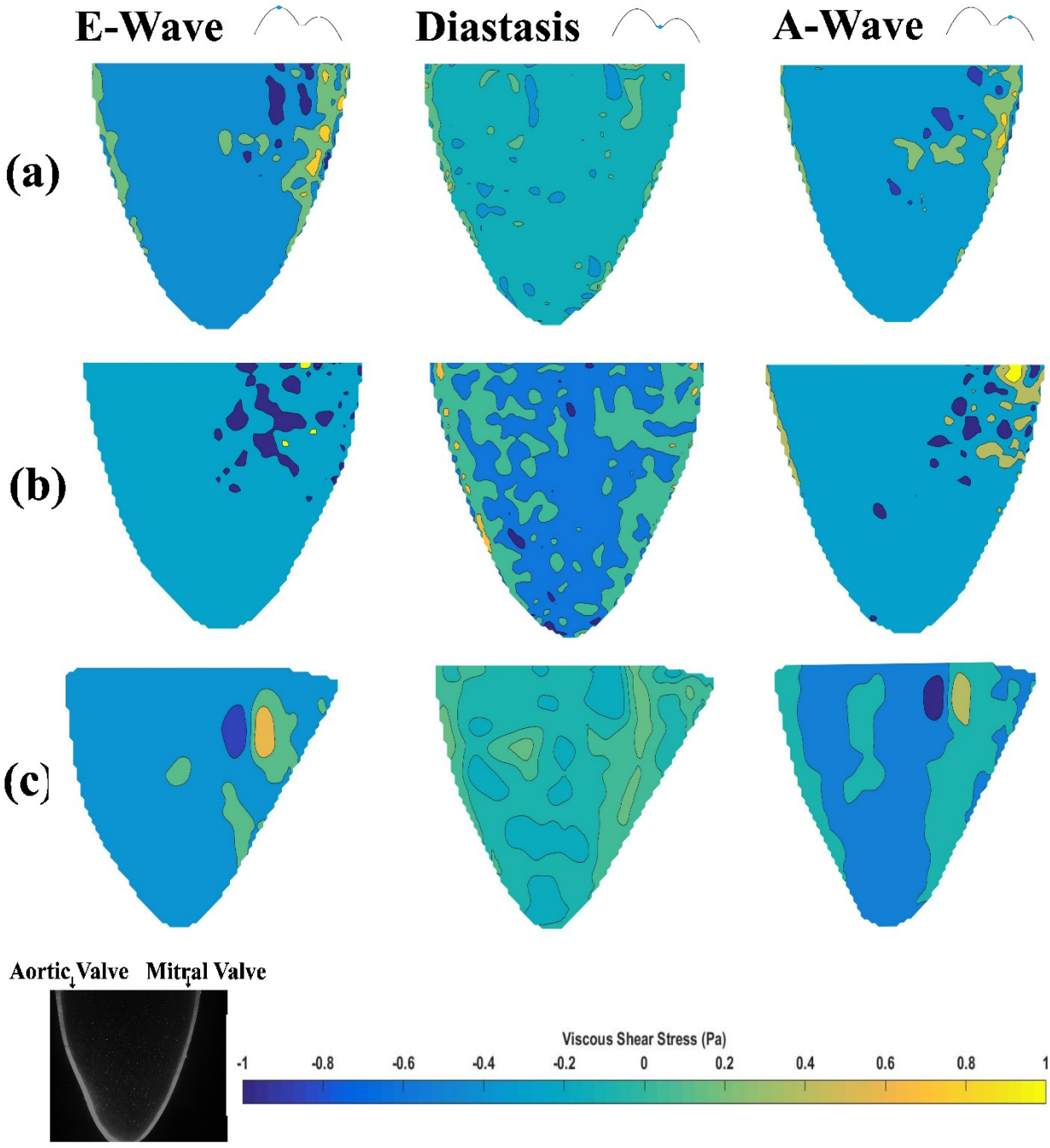

Figure 4-35 Viscous shear stress fields for (a) Normal, (b) Moderate and (c) Severe MAC cases.

Particle path

Particle paths for 8 particles during one cardiac cycle are shown for all cases (Fig. 4-36). The normal case shows particles entering the LV and leaving after one complete cycle. The particle path in this case is smooth of which particles undergo looping before leaving. The moderate case

shows a different path for the same particles. The particles pass from the entrance location through the center of the LV and out through the aortic valve. A single loop observed for half of them (four particles), and all of the particles leave after one cardiac cycle. As for the severe case, the particles reach the left ventricular wall facing the mitral valve and remain there after completing one cardiac cycle. There is one limitation for the code when dealing with LV boundaries. The bouncing of the particles reaching the left ventricular wall is not embedded in the particle tracking code yet. In the other hand, the particle tracking is sensitive to the location chosen of the particle, and a better insight for the particles behavior will be through considering all the particles in the LV.

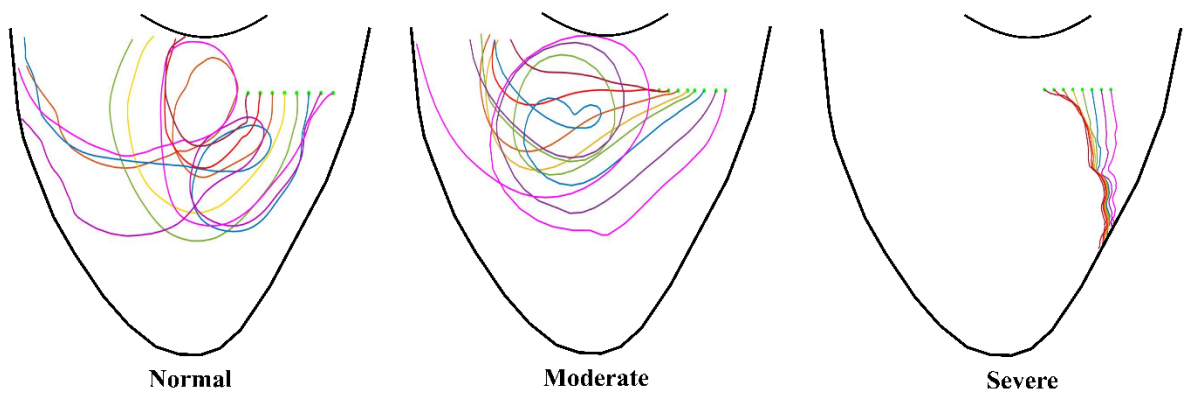

Figure 4-36 Comparison between particle path trajectories for (a) Normal, (b) Moderate and (c) Severe MAC cases.

Shear accumulation history

The importance of calculating the shear accumulation history is in the proven relation between MAC and stroke. A previous study (Benjamin et al. 1992), performed on patients with MAC, showed MAC as an independent factor doubling the risk of stroke. In return, platelet activation due to a chemical or a mechanical stimuli is one reason of stroke. A shear accumulation threshold of 3.5 Pa.s (Peterson et al. 1987) is suggested to be enough to activate the platelets which is the

first step toward thrombus formation. However, platelet activation is not an obligatory step for stroke, but it is one of the reasons.

For one cardiac cycle, the shear accumulation history was calculated for the same eight particles demonstrated in the particle path section above (Fig. 4-37). For each case, eight curves are plotted for the shear accumulation history as a function of time. In the normal case, particles show almost a linear curve throughout the time evolution. Four particles left the LV before the cardiac cycle is completed, and four left at the end of the cardiac cycle. For the moderate case, the curves is almost divided into two linear parts. The first part starts from 0 and ends at 0.15s and the second part starts from 0.15 s and ends at almost 0.36 s. The end of the curves at 0.36 s implies that all the particles took less than a complete cycle to leave the left ventricle. As for the severe case, the eight particles follow the same pattern. Comparing this graph with the particle path graph, it is clear that the particles stopping at the left ventricular wall keep on accumulating shear throughout the cycle.

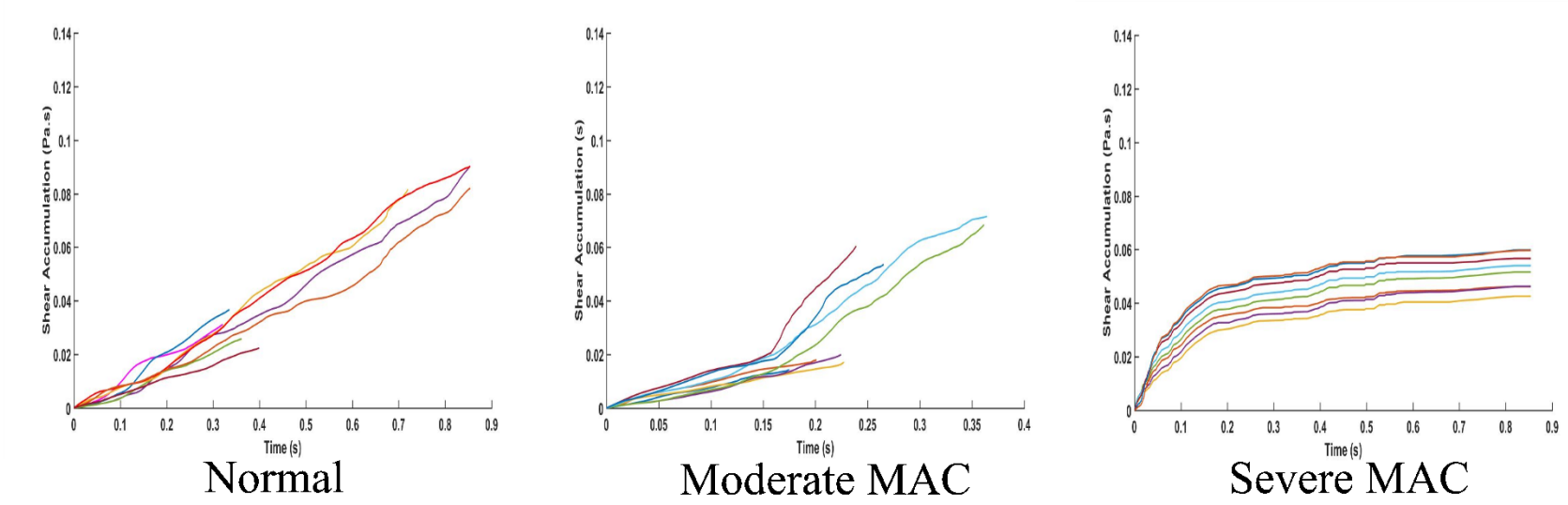

Figure 4-37 Shear accumulation history for Normal, Moderate and Severe MAC.

The maximum shear accumulated for the specified particles in the normal case is 0.089 Pa.s, while it is 0.071 Pa.s for the moderate case, and 0.059 Pa.s for the severe case. None of the cases exceed the threshold for platelet activation (3.5 Pa.s). However, the eight particles give an idea of the different patterns in the different cases, but don't cover the complete left ventricle.

Also, it should be noted that in a study made by Davies et al. 1986, it was suggested that the blood flow characteristics might be the major determinant for platelet activation rather than the magnitude of the shear stress. In other words, the cells are more sensitive to low shear stresses in turbulent flow than high shear stresses in laminar flow.

CHAPTER 5: CONCULISON & RECOMMENDATIONS

In this study, first a left heart simulator is used to conduct a fundamental study to evaluate the effect of both the severities of MAC and the orientation of a mitral valve on the left ventricle hemodynamics. Particle image velocimetry is used to obtain the velocity fields. The LV hemodynamics are then evaluated by using the velocity fields to compute vorticity, vortex formation number, viscous energy loss, viscous shear stress, particle path and shear accumulation. Results show that both severity level and orientation affect the left ventricle normal functioning through three major effects. First, increasing the energy loss and viscous shear stresses which leads to the increase in the pumping work of the LV. Second, increase in the vortex formation time beyond the optimal upper limits leading to the decrease in blood filling efficiency due to suboptimal filling through a trailing jet and not vortex ring. Third, deviation in the particle path from the optimal expected path leads to increase in shear accumulation causing an increased risk of stroke.

Future studies can further investigate, in addition to the mitral orifice area and eccentricity, the tilting effect of the MV on the severity of MAC. While there are previous studies investigating the effect of MV tilting on the LV flow patterns, there are none for MAC nor for this factor combined with mitral orifice area and eccentricity. Such an investigation can be used to suggest new parameters to redefine the severities taking into account all critical factors involved in order to help in early detection and accurate estimation of MAC. Also, further investigations have to address shear stress accumulation within a complete LV in three dimensions and covering more consecutive cycles.

Second, two patient specific valves having moderate and severe MAC are tested on the same experimental setup, along with a normal case. The same post processing procedure is followed.

Results show that MAC is not a straightforward disease. Although the maximum instantaneous velocity and vorticity is found in the severe case, the EL in the LV of moderate MAC is less than that of the severe MAC. Vortex formation time increases with the severities. Particle path is more altered than that of the normal case. It is really important to understand the meaning of those results, suggesting that MAC has two different effects depending on the calcified valve geometry. First, MAC affects the LV flow dynamics in terms of velocity, vorticity, energy loss, viscous shear stresses and VFT. The second is that MAC affects the left atrium. It is very important in this case to monitor both the left ventricle and the left atrium to avoid false interpretations using the above mentioned parameters.

Future studies can use more patient specific valves covering all severities levels to generate a database for MAC hemodynamics. This database can be used after the fluid dynamics studies of complete calcified mitral valve geometry to develop and validate new clinical parameters. A study on both the left atrium and the ventricle hemodynamics is essential to better understand the impact of this disease on the heart function.

REFERENCES

Agati, S., Cimino, G., Tonti, F., Cicogna, V., Petronilli, L., De Luca,C., Iacoboni, Pedrizzetti, G., 2014. Quantitative analysis of intraventricular blood flow dynamics by echocardiographic particle image velocimetry in patients with acutemyocardial infarction at different stages of left ventricular dysfunction. Eur Heart J Cardiovasc Imgaing. 15; 1203-1212.

Akiyama, K., Maeda, S., Matsuyama, T., Kainuma, A., Ishii, M., Naito, Y., Kinoshita, M., Hamaoka, S., Kato, H., Nakajima, Y., Nakamura, N., Itatani, K., and Sawa, T., 2017. Vector flow mapping analysis of left ventricular energetic performance in healthy adult volunteers. BMC Cardiovascular Disorders. 17; 21.

Arefin, M.S., Morsi, Y.S., 2014. Fluid structure interaction (FSI) simulation of the left ventricle (LV) during the early filling wave (E-wave), diastasis and atrial contraction wave (A-wave). Australas Phys Eng Sci Med. 37; 413–423.

Aronow, W.S., Kronzon, I., 1987. Correlation of prevalence and severity of mitral regurgitation and mitral stenosis determined by Doppler echocardiography with physical signs of mitral regurgitation and mitral stenosis in 100 patients aged 62 to 100 years with mitral anular calcium. Am J Cardiol. 60; 1189-1190.

Balta, S., Demirkol, S., Cakar, M., Kurt, O., Unlu, M., Kucuk, U., 2013. Mean platelet volume and mitral annular calcification. Blood Coagulation & Fibrinolysis. 24; 899.

Barasch, E., Gottdiener, J.S., Larsen, E.K., Chaves, P.H., Newman, A.B., Manolio, T.A., 2006. Clinical significance of calcification of the fibrous skeleton of the heart and aortosclerosis in community dwelling elderly. The Cardiovascular Health Study (CHS). Am Heart J. 151; 39-47.

Bath, P., Algert, C., Chapman, N., Neal, B., 2004. Association of Mean Platelet Volume with Risk of Stroke among 3134 Individuals with History of Cerebrovascular Disease. Arterioscler Thromb Vasc Biol. 31; 1215-1218.

Baumgartner, H., Hung, J., Bermejo, J., Chambers, J.B., Evangelista, A., Griffin, B.P., Iung, B., Otto, C.M., Pellikka, P.A., Quiñones, M. 2009. Echocardiographic assessment of valve stenosis: EAE/ASE recommendations for clinical practice. J Am Soc Echocardiogr. 22; 1-23.

Bellhouse, B.J., Talbot L., 1969. The fluid mechanics of the aortic valve. J Fluid Mech Digit Arch. 35; 721–735.

Belohlavek, M., 2012. Vortex formation time: an emerging echocardiographic index of left ventricular filling efficiency. Eur Heart J Cardiovasc Imaging. 13; 367–369.

Belohlavek, M., Jiamsripong, P., Calleja, A.M., McMahon, E.M., Maarouf, C.L., Kokjohn, T.A., Chaffin, T.L., Vedders, L.J., Garami, Z., Beach, T.G., Sabbagh, M.N., Roher, A.E., 2009. Patients with Alzheimer disease have altered transmitral flow: echocardiographic analysis of the vortex formation time. J Ultrasound Med. 28; 1493–1500.

Benjamin, E.J., Plehn, J.F., D'Agostino, R.B., Belanger, A.J., Comai, K., Fuller, D.L., Wolf, P.A., Levy, D., 1992. Mitral Annular Calcification and the Risk of Stroke in an Elderly Cohort. N Engl J Med. 327; 374-379.

Bolger, AF., Heiberg, E., Karlsson, M., Wigstrom, L., Engvall, J., Sigfridsson, A., Ebbers, T., Kvitting, J.P., Carlhäl,l C.J., Wranne, B.,2007. Transit of blood flow through the human left ventricle mapped by cardiovascular magnetic resonance. J Cardiovasc Magn Reson. 9; 741–747.

d'Alessandro, C., Vistarini, N., Aubert, S., Jault, F., Acar, C., Pavie, A., Gandjbakhch, I., 2007. Mitral annulus calcification: determinants of repair feasibility, early and late surgical outcome. Eur J Cardiothorac Surg. 32; 596.

Davies, P.F., Remuzzi, A., Gordon, E.J., Dewey, C.F., Gimbrone, M.A., 1986. Turbulent Fluid Shear Stress Induces Vascular Endothelial Cell Turnover in vitro. Proc. Natl. Acad. Sci. USA. 83; 2114-2117.

Domenichini, F., Querzoli, G., Cenedese, A., Pedrizzetti, G., 2006. Combined experimental and numerical analysis of the flow structure into the left ventricle. J Biomech. 40; 1988-94.

Elsayed, A.M., Mohamed, G.A., 2017. Mean platelet volume and mean platelet volume/platelet count ratio as a risk stratification tool in the assessment of severity of acute ischemic stroke. Alexandria Journal of Medicine. 53; 67–70.

Etebari, A., Vlachos, P.P., 2005. Improvements on the accuracy of derivative estimation from DPIV velocity measurements. Experiments in Fluids. 39; 1040-1050.

Falahatpisheh, A., Kheradvar, A., 2012. High-speed particle image velocimetry to assess cardiac fluid dynamics in vitro: From performance to validation. European Journal of Mechanics B/Fluids. 35; 2–8.

Feindel, C.M, Tufail, Z., David, T.E, Ivanov, J., Armstrong, S., 2003. Mitral valve surgery in patients with extensive calcification of the mitral annulus. J Thorac Cardiovasc Surg. 126; 777-782.

Fox, C.S., Vasan, R.S., Parise, H., Levy, D., O'Donnell, C.J., D'Agostino, R.B., Benjamin, E.J., 2003. Mitral annular calcification predicts cardiovascular morbidity and mortality: the Framingham Heart Study. Circulation.107; 1492-1496.

Fulkerson, P.K., Beaver, B.M., Auseon, J.C., Graber, H.L., 1979. Calcification of the mitral annulus: Etiology, clinical associations, complications and therapy. The American Journal of Medicine. 66; 967-977.

Fulkerson, P.K., Beaver, B.M., Auseon, J.C., Graber, H.L., 1979. Calcification of the mitral annulus: etiology, clinical associations, complications and therapy. Am J Med. 66; 967-977.

Garcia, D., Del Alamo, J.C., Tanne, D., Yotti, R., Cortina, C., Bertrand, E., Rieu, R., Fernandez-Aviles, F., Bermejo, J., 2010. Two-dimensional intraventricular flow mapping by digital processing conventional color-Doppler echocardiography images. IEEE Trans Med Imaging. 29; 1701–1713.

Gasparyan, AY., Ayvazyan, L., Mikhailidi, D.P., Kitas, G.D., 2011 .Mean Platelet Volume: A Link between Thrombosis and Inflammation. Current Pharmaceutical Design. 17; 47-58.

Gharib, M., Rambod, E., Kheradvar, A., Sahn, D.J., Dabiri, J.O., 2006. Optimal vortex formation as an index of cardiac health. Proc Natl Acad Sci U S A. 103; 6305-8.

Ghosh, E., Kovacs, S.J, 2013. The vortex formation time to diastolic function relation: assessment of pseudonormalized versus normal filling. Physiol Rep. 1; e00170.

Ghosh, E., Shmuylovich, L., Kovacs, SJ., 2009. Determination of early diastolic LV vortex formation time (T*) via the PDF formalism: a kinematic model of filling. Conf Proc IEEE Eng Med Biol Soc. 2009; 2883-2886.

Gulati, A., Chan, C., Duncan, A., Raza, S., Kilner, P.J., Pepper, J., 2011. Multimodality cardiac imaging in the evaluation of mitral annular caseous calcification. Circulation. 123; e1-e2.

Harpaz, D., Auerbach, I., Vered, Z.,Motro, M., Tobar, A., Rosenblatt, S., 2001. Caseous calcification of the mitral annulus: a neglected, unrecognized diagnosis. J Am Soc Echocardiogr. 4; 825.

Harris, J., 2012. Investigation of relative importance of some error sources in particle Image velocimetry.

Hayashi, T., Itatani, K., Inuzuka, R., Shimizu, N., Shindo, T., Hirata, Y., Miyaji, K., 2014. Dissipative energy loss within the left ventricle detected by vector flow mapping in children: Normal values and effects of age and heart rate. J Cardiol. 66; 403-410.

Honda, T., Itatani, K., Takanashi, M., Mineo, E., Kitagawa, A., Ando, H., Kimura, S., Nakahata, Y., Oka, N., Miyaji, K., and Ishii, M., 2014. Quantitative evaluation of

hemodynamics in the Fontan circulation: a cross-sectional study measuring energy loss in vivo. Pediatr Cardiol. 35; 361–367.

Itatani, K., 2014. When the blood flow becomes bright. Eur Heart J. 35; 747-752a.

Itatani, K., Okada, T., Uejima, T., Tanaka, T., Ono, M., Miyaji, K., Takenaka, K., 2013. Intraventricular Flow Velocity Vector Visualization Based on the Continuity Equation and Measurements of Vorticity and Wall Shear Stress. Jpn J Appl Phys. 52; 07HF16.

Jiamsripong, P., Calleja, A.M., Alharthi M.S., Dzsinich, M., McMahon, E.M., Heys, J.J., Milano, M., Sengupta, P.P., Khandheria, B.K., Belohlavek, M., 2009. Impact of Acute Moderate Elevation in Left Ventricular Afterload on Diastolic Transmitral Flow Efficiency: Analysis by Vortex Formation Time. J Am Soc Echocardiogr. 22; 427–431.

Kanjanauthaia, S., Nasirb, K., Katzc, R., Riverad, J.J., Takasue, J., Blumenthald, R.S., Eng, J., Budoffe, M.J., 2010. Relationships of mitral annular calcification to cardiovascular risk factors: The Multi-Ethnic Study of Atherosclerosis (MESA). Atherosclerosis. 213; 558–562.

Keane, R.D., Adrian, R.J., 1990. Optimization of particle image velocimeters. I. Double pulsed systems. Meas Sci Technol 1; 1202-1215.

Kheradvar, A., Falahatpisheh, A., 2012. The effects of dynamic saddle annulus and leaflet length on transmitral flow pattern and leaflet stress of a bi-leaflet bioprosthetic mitral valve. J Heart Valve Dis. 21; 225-233.

Kheradvar, A., Pedrizzetti, G., 2012. Vortex Formation in the Cardiovascular System. First Edition. Springer-Verlag London.

Kilner, P.J., Yang, G.Z., Wilkes, A.J., Mohiaddin, R.H., Firmin, D.N., Yacoub, M.H., 2000. Asymmetric redirection of flow through the heart. Nature. 404; 759– 761.

Kim, W.Y., Bisgaard, T., Nielsen, S.L., Poulsen, J.K., Pedersen, E.M., Hasenkam, J.M., Yoganathan, A.P., 1994. Two-dimensional mitral flow velocity profiles in pig models using epicardial echo Doppler cardiography. J Am Coll Cardiol. 24; 532–545.

Kim, W.Y., Walker, P.G., Pedersen, E.M., Poulsen, P.K., Oyre, S., Houlind, K., Yoganathan, A.P., 1995. Left ventricular blood flow patterns in normal subjects: a quantitative analysis by three-dimensional magnetic resonance velocity mapping. J Am Coll Cardiol. 26; 224–238.

Labovitz A.J, Nelson, J.G, Windhorst, D.M., Kennedy, H.L., Williams, G.A., 1985. Frequency of mitral valve dysfunction from mitral anular calcium as detected by Doppler echocardiography. Am J Cardiol. 55; 133-137.

Li, C.M., Bai1, W.J., Liu, Y.T., Tang, H., Rao, L., 2017. Dissipative energy loss within the left ventricle detected by vector flow mapping in diabetic patients with controlled and uncontrolled blood glucose levels. Int J Cardiovasc Imaging. 33; 1151-1158.

Maragiannis, D., Alvarez, P.A, C. Schutt, R., Chin, K., Buergler, J,M., Little, S.H., Shah, D.J., Nagueh., S.F, 2016. Vortex Formation Time Index in Patients with Hypertrophic Cardiomyopathy. JACC: Cardiovascular Imaging. 9; 1228- 1231.

Mayda-Domaç, F., Misirli, H., Yilmaz, M., 2010. Prognostic role of mean platelet volume and platelet count in ischemic and hemorrhagic stroke. J Stroke Cerebrovasc Dis. 19; 66-72.

McCormick, M.E., Manduchi, E., Witschey, W.R.T., Gorman, R.C., Gorman, J.H., Jiang, Y.Z., Stoeckert, C.G., Barker, A.J., Markl, M., Davies, P.F., 2016. Integrated Regional Cardiac Hemodynamic Imaging and RNA Sequencing Reveal Corresponding Heterogeneity of Ventricular Wall Shear Stress and Endocardial Transcriptome. J Am Heart Assoc. 5; e003170.

Movahed, M.R., Saito, Y., Ahmadi-Kashani, M., Ebrahimi, R., 2007. Mitral Annulus Calcification is associated with valvular and cardiac structural abnormalities. Cardiovasc Ultrasound. 5; 14.

Nishio, S., 2008. Uncertainty Analysis: Particle Imaging Velocimetry (PIV). ITTC – Recommended Procedures and Guidelines.

Osterberger, L.E., Goldstein, S., Khaja, F., Lakier, J.B., 1981. Functional mitral stenosis in patients with massive mitral annular calcification. Circulation. 64; 472-476.

Pasipoularides, A., Vlachos, P.P., Little, W.C., 2015. Vortex formation time is not an index of ventricular function. J Cardiovasc Transl Res. 8; 54-8.

Pedrizzetti, G., Domenichini, F., 2005. Nature optimizes the swirling flow in the human left ventricle. PHYS Rev Lett. 95; 108101.

Peterson, D.M., Stathopoulos, N.A., Giorgio, T.D., Hellums, J.D., Moake, J.L., 1987.Shear-induced platelet aggregation requires von Willebrand factor and platelet membrane glycoproteins Ib and IIb-IIIa. Blood. 69; 625-628.

Poh, K.K., Lee, L.C., Shen, L., Chong, E., Tan, Y.L., Chai, P., Yeo, TC., Wood, M.J., 2012. Left ventricular fluid dynamics in heart failure: echocardiographic measurement and utilities of vortex formation time. Eur Heart J Cardiovasc Imaging. 13; 385-93.

Pressman, G.S., Agarwal, A., Braitman, L.E., Muddassir, S.S., 2010. Mitral Annular Calcium Causing Mitral Stenosis. Am J Cardiol. 105; 389 –391.

Reul, H., Talukder, N., Muller, W., 1981. Fluid mechanics of the natural mitral valve. J Biomech. 14; 361–372.

Roelandt, J., 1982. Doppler Ultrasound in Cardiology: Physical Principles and Clinical Applications. International Journal of Cardiology. 5: 125-126.

Rupa‐Matysek, J., Gil, L., Wojtasinska, E., Ciepłuch, K., Lewandowska, M., Komarnicki, M., 2014. The relationship between mean platelet volume and thrombosis recurrence in patients diagnosed with antiphospholipid syndrome. Rheumatol Int. 34; 1599–1605.

Sheriff, J., Soares, J.S., Xenos, M., Jesty, J., Bluestein, D., 2013. Evaluation of shear-induced platelet activation models under constant and dynamic shear stress loading conditions relevant to devices. Ann Biomed Eng. 41; 1279-1296.

Soeki, T., Fukuda, N., Shinohara, H., Sakabe, K., Onose, Y., Sawada, Y., Tamura, Y., 2002. Mitral inflow and mitral annular motion velocities in patients with mitral annular calcification: evaluation by pulsed Doppler echocardiography and pulsed Doppler tissue imaging. Eur J Echocardiogr. 3; 128-34.

Stewart, K.C., Charonko, J.C., Niebel, C.L., Little, W.C., Vlachos, P.P., 2012. Left ventricle filling vortex formation is unaffected by diastolic impairment. American Journal of Physiology. Heart and Circulatory Physiology. 303; H1255–H1262.

Stewart, K.C., Kumar, R., Charonko, J.J., Ohara, T., Vlachos, P.P., Little, W.C., 2011. Evaluation of LV diastolic function from color Mmode echocardiography. JACC. Cardiovascular Imaging. 4; 37–46.

Stugaard, M., Koriyama, H., Katsuki, K., Masuda, K., Asanuma, T., Takeda, Y., Sakata, Y., Itatani, K., Nakatani, S., 2015. Energy loss in the left ventricle obtained by vector flow mapping as a new quantitative measure of severity of aortic regurgitation: a combined experimental and clinical study. Eur Heart J Cardiovasc Imaging. 16; 723-30.

Sutton, M.G., Tajik, A.J., Gibson, D.G., Brown, D.J., Seward, J.B., Guiliani, E.R., 1978. Echocardiographic assessment of left ventricular filling and septal and posterior wall dynamics in idiopathic hypertrophic subaortic stenosis. Circulation. 57; 512-20.

Tanné, D., Bertrand, E., Kadem, L., Pibarot, P., Rieu., R. 2009. Assessment of left heart and pulmonary circulation flow dynamics by a new pulsed mock circulatory system. Experiments in Fluids. 48; 837–850.

Varol, E., Aksoy, F., Ozaydin, M., Erdogan, D., Dogan, A., 2013. Relationship between mean platelet volume and mitral annular calcification. Blood Coagul Fibrinolysis. 24; 189-93.

Waite, L., Fine, J. M. 2007. Applied biofluid mechanics. First edition. The McGraw-Hill Companies,Inc.

Watanabe, H., Sugiura, S., Hisada, T., 2008. The looped heart does not save energy by maintaining the momentum of blood flowing in the ventricle. Am J Physiol Heart Circ Physiol. 294; H2191-2196.

Widmaier, E.P., Raff, H., Strang, K.T., 2003. Vander, Sherman, Luciano's Human Physiology: The Mechanisms of Body Function. Second edition. Mcgraw-Hill Ryerson.

Yin, W., Alemu, Y., Affeld, K., Jesty, J., Bluestein, D., 2004. Flow-induced platelet activation in bileaflet and monoleaflet mechanical heart valves. Annals of biomedical engineering. 32; 1058-1066.

Yoganathan, A.P., He, Z., Jones, S.C, 2004. Fluid Mechanics of Heart Valves. Annu. Rev. Biomed. Eng. 6; 331- 362.

Zhang, H., Liu, L., Chen, L., Ma, N., Zhou, L., Liu, Y., Li, Z., Liu, C., Hou, R., Zhu, S., 2013. The evolution of intraventricular vortex during ejection studied by using vector flow mapping. Echocardiogr. 30; 27–36.

Zhang, H., Zhang, J., Zhu, X., Chen, L., Liu, L., Duan, Y., Yu, M., Zhou, X., Zhu, T., Zhu, M., Li, H., 2012. The left ventricular intracavitary vortex during the isovolumic contraction period as detected by vector flow mapping. Echocardiogr. 29; 579–587.

Zhang, J.N., Bergeron, A.L., Yu, Q., Sun, C., McBride, L., Bray, P.F., Dong, J.F., 2003. Duration of exposure to high fluid shear stress is critical in shear-induced platelet activation-aggregation. Thromb Haemost. 90; 672-678.

Zhang, Q., Gao, B., Chang, Y., 2017. Computational Analysis of Intra-Ventricular Flow Pattern under Partial and Full Support of BJUT-II VAD. Med Sci Monit. 23; 1043-1054.

Zhong, Y., Liu, Y., Wu, T., Song, H., Zhu, Z.H.W., Cai, Y., Zhang, W., Bai, W., Tang, H., Rao, L., 2016. Assessment of left ventricular dissipative energy loss by vector flow mapping in patients with end-stage renal disease. J Ultrasound Med. 35; 965–973.

REFERENCES for Figures

1- http://www.texasheart.org/HIC/Anatomy/anatomy2.cfm
2- http://www.keywordsuggests.com/udlJBknNsGdl*sYs8AsY47uSt9ujXVWZEKjvGROQbzE
3- http://www.mayoclinic.org/
4- http://www.heart-valve-surgery.com/heart-surgery-blog/2008/02/16/mitral-valve-calcification-pictures-symptoms-treatment/
5- https://www.quora.com/Why-is-bicuspid-valve-called-mitral-valve
6- http://www.mayoclinic.org/diseases-conditions/aortic-valve-disease/ovc-20304912
7- https://www.biosciencetechnology.com/news/2015/11/google-aha-partner-investment-heart-disease-research
8- http://professional.sjm.com/resources/heart-valve-modelnumbers/~/link.aspx?_id=0d30b17f9b12496cbe01de9459082f8e&_z=z

APPENDIX A

Measuring the area of a complex shape was established by several steps. The first step was to create image contrast in the 3D patient specific valve between the orifice area (opening of the valve), and the rest of the valve. This was accomplished by using white nail polish for the body of the valve, and black pigment stamp pad for the orifice area of the valve. This step was done manually. In this step, the 3D STL files of the valves were used to better distinguish the boundaries of the opening for each valve.

A code was developed to calculate the orifice area using MATLAB. The code starts by changing the RGB images into black and white images, saving the matrix as a parameter. After that, the number of pixels presenting the orifice area is calculated through counting the number of pixels having 0 values (zero is black, 1 is white). Then, the number is converted from pixels squared to cm^2 (Fig. 1) using a reference line.

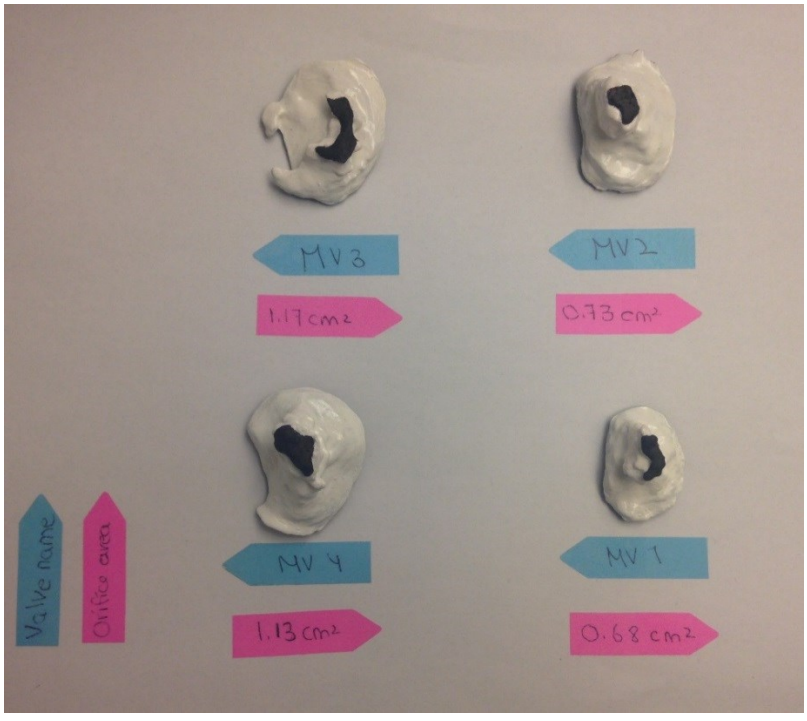

Figure A-1 Areas of the 3D printed mitral valves.